https://doi.org/10.5194/essd-2026-651
Preprint. Discussion started: 25 August 2026

Open Access Earth System Science Data Discussions

A Compilation of Marine Photosynthesis–Irradiance Data from ^{14}C Incubation Experiments

Mohammad M. Amirian[*1, 2], Emmanuel Devred[3], Stephanie Clay[3], Zoe V. Finkel[4], and Andrew J. Irwin[2]

[1]New York City College of Technology, City University of New York, Brooklyn, NY, USA
[2]Department of Mathematics and Statistics, Dalhousie University, Halifax NS
[3]Fisheries and Oceans Canada, Bedford Institute of Oceanography, Dartmouth NS
[4]Department of Oceanography, Dalhousie University, Halifax NS

*** Correspondence:** Mohammad M. Amirian; email: m.amirianmatlob@dal.ca

Abstract

Photosynthesis-irradiance (PI) experiments that measure the uptake of ^{14}C labelled bicarbonate over a light gradient established in an incubator are foundational to computations of primary productivity and models of photosynthesis in ecosystem models. We present a compilation of PI data collected over the last 50 years with largely consistent methods, totalling 3751 PI curves from the North Atlantic (2384 curves), Arctic (1209), North Pacific (90) and Indian (68) oceans. Unlike many compilations, we present original measurements of photosynthetic rate and irradiance, together with derived photosynthesis-irradiance (PI) model parameters as well as detailed metadata including experimental design, environmental conditions, and methodological variation. Using this database and a suite of PI models, we show how parameter estimates typically vary across observations and model formulations, and demonstrate how differences in experimental design and methodology can systematically affect parameter values. We show that quality statistical conversion of parameter values from one model to another is often possible, although direct estimation of parameters from original data is always preferable.

Keywords: ^{14}C Photosynthesis-irradiance data, Photosynthetic Rate, Ocean, Phytoplankton

Short summary: We compiled 50 years of measurements describing how marine phytoplankton photosynthesis responds to light, covering the North Atlantic, Arctic, North Pacific, and Indian oceans. The database provides original measurements alongside environmental and experimental information. Our analyses show that photosynthetic parameters depend on both the mathematical model and experimental methods, highlighting the value of preserving original measurements for future research.

1 Introduction

The ocean plays a central role in regulating Earth's climate by absorbing atmospheric carbon dioxide and redistributing carbon through physical, chemical and biological processes DeVries (2022); McKinley et al. (2017). Marine phytoplankton are responsible for approximately half of global primary production and form the foundation of marine food webs Field et al. (1998). As the primary producers of the ocean, they drive marine net primary production (NPP) and fuel the biological carbon pump Tréguer et al. (2018). Through photosynthetic carbon assimilation and subsequent export of organic matter to the deep ocean, phytoplankton influence atmospheric CO_2 concentrations, nutrient cycling, ecosystem productivity, and long-term climate regulation DeVries (2022); Sharoni et al. (2026). Quantifying marine primary productivity is therefore essential for understanding both present-day carbon cycling and future climate change.

Marine NPP has been estimated to be approximately 50 Pg C yr^{-1} on global scale Longhurst et al. (1995); Westberry et al. (2023), yet published estimates over the past several decades span nearly a factor of three,

https://doi.org/10.5194/essd-2026-651
Preprint. Discussion started: 25 August 2026

Open Access Earth System Science Data Discussions

ranging from 23 to 76 Pg C yr^{-1}, depending on the observational and modeling approaches employed Kulk et al. (2020); Sathyendranath et al. (2020); Tagliabue et al. (2021) . Such a large range of NPP estimates complicates the detection of long-term trends and limits confidence in projections of future marine productivity under climate change (IPCC IPCC (2021), Ch. 2, Section 2.3.4.2.2). Therefore, identifying the origin of this variability among estimates is of critical importance. Although differences among global NPP estimates are often attributed to incomplete understanding of ocean physics, ecosystem dynamics, and biogeochemical processes, substantial variation also arises from sparse observational coverage, heterogeneous experimental methodologies, differences in data processing and scaling approaches, and structural differences among the mathematical parameterizations used to represent photosynthesis.

Marine NPP models ultimately rely on representations of how phytoplankton photosynthesis responds to irradiance Kam et al. (2026); Kovač et al. (2018); Platt and Sathyendranath (1988) and environmental conditions Amirian et al. (2022); Behrenfeld and Falkowski (1997); Devred et al. (2025). Since photosynthetic rates cannot be measured continuously at basin to global scales, they are often estimated using photosynthesis–irradiance (PI) relationships derived from ^{14}C incubation experiments. These experiments provide empirical estimates of photosynthetic parameters, including the maximum photosynthetic rate (P_{max}), the initial light-limited slope (α) Britten et al. (2025); Kovač et al. (2017), and the photoinhibition rate (β) Amirian et al. (2025b), which together characterize phytoplankton photosynthetic responses to irradiance Croteau et al. (2025); Finkel (2001), providing the basis for scaling discrete experimental observations to regional and global estimates of marine primary productivity. Consequently, uncertainty in or mis-estimation of PI parameter values propagate directly into uncertainty in NPP estimates and, by extension, into estimates of ocean carbon export and climate state.

PI data have been collected across a wide range of oceanographic programs, cruises, and laboratory studies over several decades Bouman et al. (2018); Everett and Doblin (2015); Fragoso et al. (2017); Gallegos (2012); Gasol et al. (2016); Kovač et al. (2026); Kulk et al. (2020); Mattei and Scardi (2021); Westwood et al. (2011). However, these observations remain difficult to integrate consistently because experimental methodologies have evolved substantially through time. Incubation duration, light sources, irradiance resolution, temperature control, chlorophyll normalization, and phytoplankton size fractionation differ among studies, which could systematically influence derived PI parameters. Many compilations report only fitted parameter values while omitting the underlying raw observations and methodological details required for reproducible reanalysis Bouman et al. (2018); Fragoso et al. (2017); Kulk et al. (2020). Numerous empirical PI models have been proposed to represent light-limited photosynthesis Blackman (1905), light saturation Baly (1935); Bannister (1979); Prioul and Chartier (1977); Webb et al. (1974), and photoinhibition Amirian et al. (2025b); Fasham and Platt (1983); Neale and Richerson (1987); Peeters and Eilers (1978); Platt et al. (1980); Steele (1962). Although these formulations often use the same biological notation for parameters such as P_{max}, α, and β, the parameters are not precisely mathematically equivalent among models. This distinction is particularly important for photoinhibition models, where the mathematical representation of inhibition differs substantially. For example, the classical exponential formulation Platt et al. (1980) estimates a photoinhibition parameter (β), whereas the recently developed inverted-irradiance double-tanh model estimates the actual rate of photoinhibition Amirian et al. (2025b). Consequently, structural differences among PI formulations can introduce systematic differences in estimated parameters, complicating direct comparisons and synthesis of historical datasets even when the models describe similar physiological responses Amirianmatlob (2025). Several important efforts have previously compiled marine PI parameter estimates into global and regional databases Bouman et al. (2018); Gallegos (2012); Mattei and Scardi (2021), providing invaluable foundations for satellite productivity algorithms, ecological analyses, and Earth-system modeling studies. Substantial challenges remain, including incomplete methodological metadata, inconsistent fitting procedures, limited access to raw observations, and the absence of harmonized parameter estimation across multiple PI formulations.

Here we present a harmonized archive of more than 50 years of marine phytoplankton PI observations compiled from historical cruise reports, electronic repositories, and legacy datasets across the Northern Hemisphere, thanks to the Department of Fisheries and Oceans Canada. In contrast to many previous compilations, the archive preserves the ^{14}C incubation observations together with extensive metadata documenting experimental design, environmental conditions, and methodological provenance. We further provide

https://doi.org/10.5194/essd-2026-651
Preprint. Discussion started: 25 August 2026

Open Access Earth System Science Data Discussions

standardized parameter estimates obtained using a unified statistical framework implemented through the piCurve package Amirian and Irwin (2025) for 7 published photoinhibited PI model formulations developed between 1905 and 2025. In addition, the dataset includes photoinhibition diagnostics, including estimates of photoinhibition rate (β) and the derived photoinhibition onset irradiance ($P_{\max}/\beta$). Combining raw observations, harmonized parameter estimation, and methodological metadata within a reproducible framework, this archive provides a foundation for quantifying uncertainty in marine primary productivity estimates, evaluating methodological biases in historical experiments, benchmarking satellite- and machine learning–based productivity models, and supporting the development of physiologically consistent representations of phytoplankton photosynthesis in Earth system models. As an example application, we use the double-tanh formulation, identified here as the best-performing PI model Amirian et al. (2025b), as a common reference framework to evaluate the effects of thermal artifacts, incubation duration, and size fractionation on estimated photosynthetic parameters. We introduce a model-consistent harmonization framework that maps parameters derived from disparate PI formulations onto a unified parameter space defined by the double-tanh representation. This approach enables the integration of external datasets for which the underlying raw PI observations are unavailable, while minimizing structural inconsistencies introduced by differences among fitted PI models and thereby reducing artificial numerical variability in large-scale syntheses.

2 Methods & Materials

Photosynthesis-irradiance (PI) incubation experiments measuring the amount of ^{14}C-labeled bicarbonate incorporated into particulate organic carbon during photosynthesis per unit chlorophyll a (mg C (mg chl-a)$^{-1}$ d^{-1}) as a function of incident irradiance (W m^{-2}) have been performed regularly for more than five decades by scientists at the Bedford Institute of Oceanography (BIO, Department of Fisheries and Oceans Canada) using essentially the same methods (Table. 1). Although the general experimental framework remained consistent over time, some methodological details varied among campaigns including incubation duration, irradiance configuration, and light source characteristics (2.1). We compiled PI data from experiments performed at sea or from water collected at nearby time-series stations from 1972 through 2022. Typically samples were taken from two depths at each station, representing the community from the near surface and chlorophyll-a maximum. Data were collected from cruise reports published by the BIO and from internally produced electronic data compilations. An overview of each sampling campaign is in Tables. 1 & 2.

Several ancillary variables were observed at the time of sampling, grouped into three main categories: methodological, environmental, and biological. Location data (date, latitude, longitude, and sampling depth) are available for all incubation experiments. Methodological variables were the incubation temperature (°C), type of incubation light source, incubation duration, time of day samples were collected, and if samples were size-fractionated, whereby the phytoplankton community was separated into discrete size classes using membrane filtration (e.g., >1 or <1 μm & >3 or <3 μm & >5 or <5 μm). Environmental variables include *in situ* sample temperature, salinity, sea-surface photosynthetically active radiation (PAR), and dissolved inorganic nutrients (nitrate, nitrite, ammonia, phosphate, and silicate). Biological variables include chlorophyll a concentration and particulate carbon and nitrogen. The following summarizes the protocols employed by the studies contributing to the database, and the compiled database is available through zenodo https://doi.org/10.5281/zenodo.21908199, Amirian et al. (2026).

2.1 Experimental protocols

Photosynthesis-irradiance experiments. Photosynthesis–irradiance (PI) incubation experiments were conducted using the ^{14}C tracer method following Strickland and Parsons Strickland and Parsons (1972). Seawater samples were collected from discrete depths (typically two per station) and dispensed into replicate light and dark bottles. For light-saturation experiments, between ∼20 and 42 light bottles and 2–3 dark bottles were inoculated with $NaH^{14}CO_3$ (typically ∼5–25 μCi per experiment, or ∼1 mL spike per bottle depending on protocol year). Bottles were incubated for 0.5 to 4 h in temperature-controlled deck incubators supplied with flowing seawater to maintain near *in situ* conditions. Irradiance gradients were generated using artificial light sources, including 150 W floodlights (e.g., GTE Sylvania PAR 150), higher-intensity tungsten–halogen lamps (up to 2000 W), and halogen reflector (MR16 50 W) with bottle positions arranged

https://doi.org/10.5194/essd-2026-651
Preprint. Discussion started: 25 August 2026

Open Access Earth System Science Data Discussions

to span sub-saturating to supra-saturating light levels. Maximum (artificial) irradiance levels inside the incubators ranged from 50 to ∼1,360 W m^{-2}, with a median of 462 W m^{-2} and an interquartile range of 327–630 W m^{-2}, depending on configuration and experiment. Incident irradiance within incubators was quantified using pyranometers, and spectral characteristics were occasionally measured with spectroradiometers. Photosynthetically active radiation, PAR, (400–700 nm) was occasionally measured using a quantum sensor.

At the end of incubation, samples were filtered immediately onto 25 mm diameter membrane filters (typically 0.45 μm pore size). Filters were dried, exposed to HCl fumes to remove inorganic ^{14}C, and radioactivity was quantified using liquid scintillation counting. In some cases, filters were stored frozen prior to acidification and counting. Carbon fixation rates were calculated from disintegrations per minute (DPM) following standard protocols and normalized to chlorophyll-*a* concentration to yield biomass-specific photosynthetic rates.

For size-fractionation experiments, three samples were collected at each station. One sample was analyzed as the whole phytoplankton community, while the remaining two were used for size-fractionation analyses. Size fractionation was achieved by sequential filtration using Nuclepore membrane filters. For the 1 μm treatment, the > 1 μm fraction consisted of material retained on a 1.0 μm pore-size Nuclepore filter, whereas the < 1 μm fraction comprised the filtrate passing through the filter. The same procedure was applied using 3 μm and 5 μm pore-size Nuclepore filters to obtain the corresponding $> 3/ < 3$ μm and $> 5/ < 5$ μm size fractions.

Environmental data. Salinity was measured using an inductively coupled conductivity salinometer (Auto-Lab), providing high-precision conductivity-based determinations of practical salinity. Incubation temperatures were controlled by pumping water from a temperature-regulated bath through the incubation system, ensuring that experimental temperatures matched *in situ* conditions except during dedicated temperature-manipulation experiments, where a range of approximately ±10 °C around ambient temperature was used to examine thermal effects on assimilation number. Photosynthetically active radiation (PAR) was also measured using a 2π quantum sensor (LI-COR LI-1905).

Nutrients. Concentrations of five dissolved inorganic nutrients (nitrate, nitrite, ammonia, phosphate, and silicate) were routinely measured for each incubation location and depth. Nutrients were determined using standard colorimetric techniques. For many early datasets, nitrate was quantified as the sum of nitrate and nitrite following reduction of nitrate to nitrite using a cadmium–amalgam column. Nitrate and nitrite were analyzed according to the classical procedures of Strickland and Parsons Strickland and Parsons (1972). Ammonia concentrations were measured with a spectrophotometer using the phenol–hypochlorite method described by Solórzano Solorzano (1969). Phosphate was determined following the molybdenum–blue method of Murphy and Riley Murphy and Riley (1962), and silicate was analyzed following the procedure of Mullin and Riley Mullin and Riley (1955). In later datasets (mostly after 1980s), samples were typically stored frozen at –20°C and analyzed later on a Technicon II AutoAnalyzer using standardized industrial methods: 155-71W for phosphate, 158-71W for nitrate, and 186-72W for silicate Irwin et al. (1989b, 1990a). Further, nutrients samples collected from the Labrador Sea were measured following collection in agreement with the method described in the GO-SHIP Repeat Hydrography Manual Becker et al. (2020). These procedures provide high analytical precision and are consistent with long-term oceanographic protocols, allowing direct comparison among decades of measurements. In our compilation, data were recorded as NA if the nutrient was not measured, was below the detection limit, or was excluded if the sample did not meet quality-control criteria.

Biological variables. Particulate carbon and particulate nitrogen were determined using standard combustion techniques. Replicate samples (typically 0.5–1 L) were filtered onto pre-combusted filters (Whatman GF/C; 2.4 cm diameter; nominal pore size ≈ 0.7–0.8 μm). Filters were gently vacuum-dried, folded in aluminum foil, and stored frozen at –20 °C until analysis. Prior to measurement, filters were freeze-dried overnight and combusted in a Hewlett-Packard Model 185B CHN analyzer to determine carbon and nitrogen content. Chlorophyll-*a* was typically quantified using the fluorometric technique of Yentsch & Menzel Yentsch and Menzel (1963), as modified by Holm-Hansen et al. Holm-Hansen et al. (1965). Following collection, duplicate samples (100 mL) were filtered onto 25 mm GF/F filters and immediately placed in 10 mL of 10% Acetone. Vials were placed for 24h in a -20 °C freezer to allow extraction. Samples were then brought to room

https://doi.org/10.5194/essd-2026-651
Preprint. Discussion started: 25 August 2026

Open Access Earth System Science Data Discussions

temperature and chlorophyll-a fluorescence was measured on a Turner-Designed fluorometer and converted into chlorophyll-a concentration using calibration coefficients derived from pure chlorophyll-a standards. The mean chlorophyll-a concentration from the two duplicates was reported.

2.2 Photosynthetic Model

The quantitative description of photosynthesis–irradiance (PI) relationships dates back to the pioneering work of Blackman Blackman (1905), who proposed a piecewise linear representation of the photosynthetic response to light. Since then, numerous mathematical formulations have been developed to describe the characteristic shape of PI curves. Under low irradiance, photosynthetic rate increases approximately linearly with light until the photosynthetic apparatus becomes light-saturated and approaches its maximum photosynthetic capacity, $P_{\max}$. In many phytoplankton species, however, photosynthesis does not immediately decline after reaching saturation. Instead, a broad plateau is commonly observed before photosynthetic rate decreases at higher irradiances because of photoinhibition, particularly in open-ocean datasets Amirianmatlob (2025). Many existing PI models fail to reproduce all three phases of the PI, namely, light limitation, light saturation, and photoinhibition Amirian et al. (2025b).

When photoinhibition is absent, light-saturating models, such as the Jassby–Platt hyperbolic tangent model Jassby and Platt (1976), provide an adequate description of the PI relationship. Historically, photoinhibition has been incorporated by multiplying a light-saturating model by an exponential decay term (see models labelled Ph02–Ph07 in Table 3). Although mathematically convenient, this formulation forces the curve to attain a single sharp maximum followed immediately by exponential decline, preventing it from reproducing the photosynthetic plateau frequently observed in experimental data. Biologically, these models implicitly assume that photoinhibitory processes begin immediately after saturation and progressively overwhelm photosynthetic capacity, effectively conflating photodamage with photoinhibition. An additional limitation is that the maximum photosynthetic rate, $P_{\max}$, is no longer estimated directly from the data. Instead, it is computed indirectly from the theoretical maximum photosynthetic rate (P_s), the initial slope (α), and the photoinhibition parameter (β), making $P_{\max}$ susceptible to error propagation and often resulting in systematic underestimation (Table. 3). Consequently, many studies have avoided this issue by excluding observations collected after the onset of photoinhibition, thereby discarding potentially valuable information on the high-light response.

Here we use the double-tanh model (Eq. 1) as our primary model for the PI curve, as it addresses all the mentioned drawbacks, accurately represents the photosynthetic plateau in the presence of photoinhibition, and reduces to the widely used Jassby–Platt tanh model Jassby and Platt (1976) when photoinhibition is not observed Amirian et al. (2025b), overcoming the aforementioned limitations. The double-tanh model is

$$P = P_{\max} \tanh\left(\frac{\alpha\, I}{P_{\max}}\right) \tanh\left[\left(\frac{P_{\max}}{\beta\, I}\right)^{\gamma}\right] + R, \qquad \gamma = \cosh^2(1) \approx 2.38 \tag{1}$$

where P is the chlorophyll-normalized photosynthetic rate (mg C (mg chl a)$^{-1}$ h^{-1}), I is the incident irradiance (W m^{-2}), $P_{\max}$ is the maximum chlorophyll-normalized photosynthetic rate (same units as P), α is the photosynthetic efficiency at low irradiance (mg C (mg chl a)$^{-1}$ h^{-1} m^2 W^{-1}), β is the photoinhibition rate controlling the decline in photosynthesis at high irradiance, and R is dark respiration rate with same units as P. We use a fixed shape parameter $\gamma = \cosh^2(1) \approx 2.38$ as this was supported by most experiments and also enabled us to estimate the rate of inhibition unlike other existing models Amirian et al. (2025b). Two derived irradiances are commonly computed from estimated PI parameters of the double-tanh (Eq. 1) model. The photoadaptation irradiance, I_α is obtained as $I = P_{\max}/\alpha$. The onset of photoinhibition is quantified by I_β and is obtained as $I = P_{\max}/\beta$. The plateau in the model is noticeable when the ratio I_β/I_α is larger than 8 Amirian et al. (2025b).

We have selected six commonly used photoinhibition models from literature in addition to the double-tanh model (Eq. 1) to investigate how parameters estimated from alternative formulations can be translated into the parameter space of the double-tanh model when the original raw ^{14}C incubation data are unavailable (Table. 3). Parameters of these models are theoretical maximum photosynthesis rate, P_s, initial slope (α), and photoinhibition parameter (β). In the absence of photoinhibition ($\beta = 0$), these formulations reduce

https://doi.org/10.5194/essd-2026-651
Preprint. Discussion started: 25 August 2026

Open Access Earth System Science Data Discussions

to light-saturating models, for which P_s corresponds directly to the maximum photosynthesis rate, $P_{\max}$. When photoinhibition is present ($\beta > 0$), however, $P_{\max}$ is no longer equal to P_s and must instead be derived numerically from a combination of all estimated parameters, as summarized in Table. 3.

2.3 Statistical analysis

All statistical parameter estimation was performed using the R package piCurve Amirian and Irwin (2025). Although we acknowledge that the spectrum of the light source inside the incubators could affect the initial slope of the PI curve Bouman et al. (2018); Kyewalyanga et al. (1997), we report PI parameters without correction to avoid propagating uncertainties. However, the spectrum of the illumination irradiance and the phytoplankton absorption spectrum can be used to standardize to a reference light source (usually a flat spectrum) and changes in the phytoplankton community, using published field-based parameterizations of chlorophyll-specific absorption Bricaud et al. (1995) integrated in the version 0.4.4 of our R package Amirian and Irwin (2025), `piCurve::absCoef`.

As light attenuates rapidly down the water column and chlorophyll-a concentration (used as a normalizing factor) changes with depth as well, all PI parameters should be expected to vary with sampling depth. We quantified the vertical variation in PI parameters. For each set of PI curves at the same location and time but gathered at different depths, differences between deeper and shallower samples were calculated, X_{deeper} - $X_{\text{shallower}}$, for each parameter. A two-sided t-test was used to quantify the mean vertical difference and test if it differed significantly from zero.

A small number of PI curves in our collection were designed to study the effect of incubation temperature, incubation duration, and size fractionation of the community sample. We highlight these experiments here to show the effect of these experimental treatments and identify them as experimental manipulations in the compiled dataset which some users of the database may want to exclude from further analysis.

In most experiments, incubation temperatures were maintained as close as possible to the original sample temperature, typically within ±1°C. Two cruises (`arc80` and `dis81`) included temperature-manipulation experiments in which, for each sample, 3-4 replicate PI incubations were conducted under identical conditions except for the incubation temperature. For each station and parameter, we calculated the relative difference in parameter values between each temperature-manipulated incubation and the corresponding reference incubation (i.e., the incubation in which the sample and incubation temperatures were approximately equal). The relative difference was computed using the following expression:

$$\text{Relative Difference} = \frac{X_{tmi} - X_{ref}}{X_{ref}} \tag{2}$$

where X_{tmi} is the PI parameter estimated from a temperature-manipulated incubation and Xref is the parameter estimated from the reference temperature-matched incubation.

Two cruises (`ung79` in 1979 and `bb80` in 1980) reported PI curves for replicate samples conducted for multiple incubation durations (0.5, 1, 2, 3, and 4 h). The majority of incubations in the rest of the dataset were conducted for 3 h. The highest incubation duration, 4 hour, were used as the reference baseline and deviations in photosynthetic parameters at shorter incubation times were evaluated relative to this reference. To identify replicate water samples that differ only in incubation time, data were grouped in space (latitude, longitude, and depth), according to temperature and nutrient concentration, sampling date, and local sampling time. Differences in parameter values were assessed using multivariate meta-analysis to account jointly for parameter uncertainty and inter-parameter correlation Lipsey and Wilson (2001). For each incubation group, covariance matrices of the fitted photosynthetic parameters were obtained from the inverse Hessian of the likelihood using `piCurve::InfoMat_piCurve`. Uncertainty in derived irradiances, I_α and I_β, were obtained using the delta method Oehlert (1992). Meta-analysis models were fitted using the `mvmeta::mvmeta` framework with fixed effects Gasparrini and Armstrong (2013); Gasparrini et al. (2012). Samples exhibiting detectable photoinhibition ($\beta > 0$) and those without detectable photoinhibition (β statistically 0) were analysed separately. Population-level estimates of $P_{\max}$ and α were obtained by combining these two regimes using a convex weighting based on the empirical frequency of photoinhibition across all incubations. Results

https://doi.org/10.5194/essd-2026-651
Preprint. Discussion started: 25 August 2026

Open Access Earth System Science Data Discussions

were summarized using forest plots, and residual heterogeneity was assessed using the I^2 statistic Gasparrini et al. (2012).

Seven cruises reported PI curves for samples on size fractionated samples as well as bulk community samples. We computed the relative change in PI parameters, $P_{\max}$, α, β, and derived irradiances (I_α and I_β) across size fractions using Eq. 2. Because group sample sizes were generally small (< 30) and non-normal, we estimated 95% confidence intervals for the median ratio using nonparametric bootstrapping (10,000 resamples). The cruise reports with size-fractionated samples are `dis81`, `az82`, `arc83`, `bda83`, `gbss85`, `ls85`, and `cd86` (for details on this report, see Table 1)

We examined the relationship among PI parameters and environmental variables, including temperature, nutrient concentrations (nitrate, phosphate, and silicate), and PAR using the Pearson correlation coefficient. Prior to analysis, temperature values (°C) were converted to Kelvin by adding 273.15 to permit logarithmic transformation while preserving physical meaningful scale. All variables were natural log-transformed to reduce skewness and stabilize variance. Pearson correlation coefficients were computed using the `rcorr` function in `Hmisc` R package Harrell Jr (2019), which handles missing observations through pairwise deletion. Only statistically significant correlations ($p < 0.001$) were retained for visualization and interpretation.

Effect of model formulation on PI parameters.

Photosynthesis–irradiance studies employ a wide range of models to study PI curves, and they commonly report estimated parameters rather than raw photosynthetic rate and irradiance data. Since PI formulations vary in their algebraic form, the estimated parameters across models are prone to numerical differences. As a result, when comparing different studies, it is difficult to know what variation or bias has been introduced by the change in model choice. To enable a model-consistent synthesis of PI parameters obtained from multiple models, we developed a parameter-mapping framework that translates parameters from commonly used PI models into the parameters of the double-tanh model.

Using our PI database, we fitted seven commonly used PI formulations (Table 3) to all experiments under identical statistical criteria as implemented in the R package `piCurve`, Amirian and Irwin (2025) obtaining a set of PI parameters with uncertainties for each PI curve and each model. Our goal was to determine how well the double-tanh PI parameters (Eq. 1) could be recovered from only fitted parameters from other models, listed in Table 3. For each model, double-tanh parameters were estimated as regression responses, y, with the parameters from each model as predictors, x_i ($y \sim x_i$). The theoretical maximum photosynthetic rate (P_s), rather than the derived $P_{\max}$ (i.e. $P_{\max}^{\text{ref}} \sim P_s^{\text{others}}$) was used as a predictor. Since classical photoinhibition parameterizations differ considerably in interpretation from the β parameter of the double-tanh model Amirian et al. (2025b), the double-tanh photoinhibition rate (β) was estimated using multivariate regression incorporating P_s, α, and the classical inhibition parameter, β (i.e. $\beta^{\text{ref}} \sim P_s^{\text{eq}_j} + \alpha^{\text{eq}_j} + \beta^{\text{eq}_j}$) where eq_j represents the specific model equation. All mappings were estimated using weighted least squares, and all parameters were log transformed prior to regression in order to bring the distribution of the strictly positive values of response and predictor closer together. The estimated error of the log transformed response variables, y, was calculated using delta method, i.e. $\text{SE}_{\log(y)} = \text{SE}_y / y$.

3 Results

Our data compilation comprises 3,751 individual ^{14}C photosynthesis–irradiance (PI) incubations collected between 1973 and 2022 from 822 oceanographic stations worldwide, yielding a total of 111,209 paired observations of photosynthetic rate as a function of irradiance. Samples span depths from the sea surface to 150 m and encompass 19 Longhurst biogeographical provinces Longhurst (2010), providing broad spatial and ecological coverage (Tables. 1 & 2). The dataset is dominated by observations from the Northern Hemisphere, with year-round sampling but a clear seasonal bias toward the productive months of April–August, peaking in May, which accounts for 24.7% (927 of 3,751) of all experiments. Most records were collected prior to 2020 (91.7% = 3,440 of 3,751), while the remaining 8.3% represent more recent contributions, extending the temporal range into the present decade (Fig. 1).

Ancillary environmental, biological, and methodological variables were unevenly represented across the com-

https://doi.org/10.5194/essd-2026-651
Preprint. Discussion started: 25 August 2026

Open Access Earth System Science Data Discussions

piled PI experiments (Fig. 2). Among environmental measurements, *in situ* temperature was available for most of incubations, whereas salinity, nitrite, ammonia, and PAR were reported less consistently. Nutrient measurements, particularly nitrate, phosphate, and silicate, were comparatively well represented with roughly $\sim$ 70% measured or reported. Methodological descriptors including size fractionation, incubation temperature, sampling time, incubation duration and light source characteristics were available for more than $\sim$ 65% of experiments. Most experiments were performed on whole phytoplankton communities, with only a small minority conducted on size-fractionated subsets (7%). In addition, incubation temperature deviated by less than 1°C from sample temperature in most experiments. Three main light sources were reported: a 150W floodlight (17%), a 250W tungsten–halogen lamp (27%), a 2000W tungsten–halogen lamp (22%), and MR16 50 watt Halogen Reflector (34%). Incubation duration was typically 3-4 h (85%), with some conducted over shorter periods (0.5-2h: 11%) and few cases unavailable (4%).

The compiled observations span a broad hydrographic range characteristic of diverse oceanographic environments (Fig. 3 panel A). Most samples were collected with salinities of 28-35 PSU and temperature between 0 and 18 °C, although colder, fresher and warmer water masses were also sampled. Dissolved inorganic nutrient concentrations exhibited strongly right-skewed distribution (Fig. 3 panel B), with most observations occurring at relatively low concentrations and fewer measurements extending into highly enriched conditions.

Particulate organic carbon (POC), particulate nitrogen (PON), and chlorophyll-*a* (Chla) concentrations exhibited strongly right-skewed distributions characteristic of biological and biogeochemical variables spanning oligotrophic to bloom conditions (Fig. 4). Most chlorophyll-*a* concentrations were below approximately 5 mg m^{-3}, although values exceeding 20 mg m^{-3} were occasionally observed. Particulate organic carbon concentrations were centered near $\sim$ 100 mg m^{-3} with a long upper tail extending beyond 900 mg m^{-3}, while particulate organic nitrogen was typically concentrated between $\sim$ 10 and 50 mg m^{-3}. The approximately log-normal structure of all three variables indicates that relatively low-to-moderate biomass conditions dominated the dataset, whereas highly productive bloom conditions occurred less frequently but contributed substantially to the upper tails of the distributions.

Experimental irradiance configurations varied substantially among studies and decades (Fig. 5). Maximum incubation irradiances most commonly ranged between approximately 100 and 1000 Wm^{-2}, although some experiments exceeded the upper range. Deeper samples (>25m) were generally associated with slightly lower maximum treatment irradiances than shallow samples (<25m). Sea-surface PAR were available for only a subset of incubations ranging from 0 to 800 Wm^{-2}. Zero PAR simply indicates that the samples were either taken before dawn or after sun set (Fig. 5 panel A). The number of irradiance treatments used to construct individual PI curves also varied through time, with experiments conducted during the 1970s showing substantially greater variability than more recent studies, which converged toward more standardized irradiance configurations centered around approximately 30 treatments per curve (Fig. 5 panel 5B).

PI parameters and associated derived irradiance metrics (I_α and I_β) are estimated using the double-tanh model (Eq. 1) and are approximately distributed log-normally and spanned several orders of magnitude Fig. 6. The distribution of photoinhibition rate, β, and its associated onset irradiance, I_β shows the range of photoinhibition rates and irradiances at which photoinhibition becomes quantitatively important across the PI curves in our database. The photoinhibition rate β is frequently less than 10% of the photosynthetic efficiency α, indicating that the decline in photosynthetic rate at high irradiance is more gradual than the increase at low irradiance. The ratio I_β/I_α was centered near 12 ($\log_{10} \approx 1.08$), indicating the presence of a substantial plateau region in 82% of PI curves with photoinhibition (Fig. 6).

Comparison of PI parameters across the water column revealed consistent but contrasting depth-related patterns (Fig. 7). The maximum photosynthetic rate ($P_{\max}$) decreased with increasing depth, whereas photosynthetic efficiency (α) increases with decreasing irradiance, the photoinhibition parameter (β), and dark respiration rate (R) increased. The mean depth-related difference (Δ = deep − surface) was −0.49 (95% CI: −0.59 to −0.38) for $P_{\max}$ and 0.021 (95% CI: 0.011–0.032) for R, both expressed in mg C (mg chl *a*)$^{-1}$ h^{-1}. Corresponding mean differences were 0.0061 (95% CI: 0.0024–0.0099) for α and 0.0012 (95% CI: 0.0008–0.0017) for β, both expressed in mg C (mg chl *a*)$^{-1}$ h^{-1} m^2 W^{-1}. Comparisons between parameters with the same units showed that the magnitude of the depth-related difference was approximately fivefold greater for α than for β, and approximately 23-fold greater for $P_{\max}$ than for R. The increase in β at greater depths

https://doi.org/10.5194/essd-2026-651
Preprint. Discussion started: 25 August 2026

Open Access Earth System Science Data Discussions

is consistent with low-light-acclimated phytoplankton experiencing greater photodamage when exposed to high irradiance during the ^{14}C incubation experiments.

The data reveal that the PI parameters could be strongly influenced by temperature variability when the incubator temperature deviates from in situ sample temperature (Fig. 8). The magnitude and the trend of the impact vary, depending on the conditions where the sample was taken. In dis81 with average in situ sample temperature of 18.4 °C, PI parameters declined with increasing temperature inside the incubator: $P_{\max}$ decreased significantly (slope = –0.0327 ± 0.0065 mg C mg chl a h^{-1} $°C^{-1}$, $p < 0.0001$), β also declined (slope = -0.0507 ± 0.0230 units, $p = 3.6\times10^{-2}$), and α showed no consistent trend. Temperature differences up to ~10 °C produced changes of up to ~70% in both $P_{\max}$ and β. No significant trends were observed in the derived photoacclimation irradiance I_α and photoinhibition onset irradiance I_β. In contrast, `arc80` with average in situ sample temperature of 3.4 °C exhibited a positive temperature response, with $P_{\max}$ increasing sharply (slope = 0.0987 ± 0.0049, $p < 0.0001$), β also rising significantly (slope = 0.0289 ± 0.0033, $p < 0.0001$), and α showing a more moderate but still significant increase (slope = 0.0154 ± 0.0048, $p = 2.1\times10^{-3}$). The derived irradiances were significantly impacted by incubation temperature (I_α: slope = 0.120 ± 0.0145, $p < 0.0001$ and I_β: slope = 0.075 ± 0.06, $p < 0.0001$). In this dataset (`arc80`), temperature differences up to 8 °C resulted in more than a 100% increase in Pmax, I_α & I_β, and up to ~40% increases in α and β. These contrasting patterns demonstrate if the samples were collected at low temperature, an increase in incubation temperature (compare to *in situ*) increases all PI parameters (except R), while if they were collected at higher temperature, then the impact of incubation temperature is negative. No trends were observed in the dark respiration rate, R, within these datasets.

Incubation duration, ranging from 0.5 to 4 hours, typically 2-4 hours, had no detectable effect on photosynthetic efficiency (α), whereas clear and systematic effects were observed for the other PI parameters, $P_{\max}$ and β (Fig. 9). Photoinhibition rates (β) were significantly higher in samples incubated for 4 h compared with shorter incubations, although no significant difference was detected between 3 h and 4 h. In contrast, photosynthetic capacity ($P_{\max}$) was significantly elevated in samples incubated for 2-3 h relative to the 4 h baseline, with the highest mean $P_{\max}$ observed at 3 h. The derived irradiance parameter $I_\alpha = P_{\max}/\alpha$ exhibited limited sensitivity to incubation duration, consistent with the stability of across treatments. In contrast, the photoinhibition onset irradiance I_β decreased markedly with increasing incubation duration, indicating that either higher irradiance is required to induce photoinhibition at shorter incubation times or that prolonged light exposure lowers the irradiance threshold for photoinhibitory responses.

Size fractionation produced distinct and cruise-specific shifts in photosynthetic parameters relative to whole-community samples (Fig. 10). $P_{\max}$ was consistently lower in the $< 1\mu m$ and $< 3\ \mu m$ fractions across most cruises, except for `ls85` and `az82`, where no reduction was observed. Differences in α were less common and largely restricted to cd86, where $< 1\ \mu m$ samples showed reduced α and $< 5\ \mu m$ samples exhibited elevated values. Derived photo-acclimation irradiance I_α was generally lower in size-fractionated samples, with `ls85` again the primary exception. Photoinhibition rate β was typically reduced in the < 1-5 μm fractions, although several cruises (`gbss85`, `cd86`, `az82`) showed no detectable differences. Approximately one-third of cruises exhibited significant shifts in I_β, with whole community samples generally yielding higher values except in `cd86` (whole community vs $< 5\ \mu m$), where the reverse pattern occurred. Larger fractions ($> 1\ \mu m$) showed few deviations from whole community values, aside from `dis81` (higher $P_{\max}$ and β in the fractionated samples) and `cd86` (higher α and β in community samples). Together, these results indicate that size structure can exert strong effects on PI parameters, with consistent reductions in $P_{\max}$, β, and derived irradiance metrics in the smallest fractions. Quantitative summaries of median ratios and median absolute deviations are provided in Table 4.

Across the dataset, PI parameters and derived photoacclimation irradiances exhibit structured and statistically significant covariation with environmental conditions (Pearson correlations on log–log–transformed variables; Fig. 11). Temperature is positively correlated with photosynthetic capacity ($P_{\max}$), photoinhibition (β), and derived photoadaptation irradiance (I_α), with moderate correlations ($r \approx 0.3$-0.4) and no significant correlations for α and I_β. In contrast, dissolved nutrients (NO_3^-, PO_4^{3-}, SiO_x) show predominantly negative correlations with PI parameters (in particular Phosphate and Silicate), strongest for $P_{\max}$, β, and I_α ($r \approx -0.3$) but significantly weaker for α and I_β; PAR is negatively correlated with α and positively with I_α; no significant linear association between other photosynthetic parameters and PAR is observed.

https://doi.org/10.5194/essd-2026-651
Preprint. Discussion started: 25 August 2026

Open Access Earth System Science Data Discussions

Chlorophyll-a is weakly correlated with all the parameters ($P_{\max}$, β, I_α: r = 0.1 & I_β: r = -0.1) other than where no significant linear correlation is observed. The PC and PN were weakly correlated with alpha (r = 0.1) and I_α (r = -0.1), respectively.

Linear models predicting the double-tanh PI parameters from PI parameters obtained from other models generally performed well (Fig. 12). Across all commonly-used models, all parameters, namely the maximum photosynthetic rate ($P_{\max}$), the initial slope (α), and photoinhibition rate (β), were robustly recovered, with coefficients of determination (R^2) ranging from $0.96 - 0.98$ for $P_{\max}$, 0.66-0.95 for α, and 0.66–0.75 for β. Estimated scaling coefficients for $P_{\max}$ were tightly constrained around unity (0.98-1.09), indicating near one-to-one correspondence between theoretical maximum photosynthesis rate, P_s and double-tanh representation, $P_{\max}$; α correction factors were more varied (0.61–0.88). The linear model recovery of the photoinhibition rate (β) was weaker than $P_{\max}$ and α. The lowest performance was observed for Ph07 (R^2 = 0.66), consistent with its limited capacity to represent inhibition independently of other parameters. All the estimated values were statistically significant (p-value $< 10^{-5}$) and the correction factors are listed in Table 5.

4 Discussion

Our database compiles over 3,751 photosynthesis-irradiance curves from ^{14}C incubations of natural phytoplankton samples collected over 50 years. Unlike many other data collections, we report all the original data and metadata and not simply derived PI parameters. Metadata include temperature, salinity, macronutrient concentrations, particulate carbon and nitrogen, and variations in the experimental protocol. This data compilation enables consistent and reproducible analysis of a large collection of PI curves in future projects. A small proportion of the PI curves are experimental treatments varying incubation temperature, incubation duration, or using size-fractionated samples; these experiments are discussed and flagged so that users of the database can choose whether or not to include them in their analyses. We analyze the PI data with a recently developed functional form of the PI curve that better fits most data exhibiting photoinhibition compared to previously published models. We show how PI parameters published without the benefit of the full PI data can be converted using regression models to the PI parameters for the model used in our analysis.

5 Code and Data Availability

The compiled photosynthesis–irradiance (PI) database presented in this study is publicly available through Zenodo https://doi.org/10.5281/zenodo.21908199, Amirian et al. (2026). The archive contains the compiled PI incubation data together with associated biological, environmental, and methodological metadata. Fitted P–I model parameters and associated statistical metrics used in the analysis are available separately through Zenodo https://doi.org/10.5281/zenodo.16748102, Amirian et al. (2025a) and are described in Ref Amirian et al. (2025b).

Statistical analyses were conducted using the `piCurve` R package, Version 0.4.5, which provides functions for fitting and evaluating PI models. The software is open source and described in Ref Amirian and Irwin (2025). The database, derived parameter estimates, and software are therefore archived separately to allow independent access, citation, and reuse.

Author contribution

MMA led the project, compiled and curated the data, developed the methodology and software, performed the formal statistical analyses and visualizations, and prepared the initial manuscript draft. ED provided the original data and contributed scientific guidance. SC curated the data. ZVF contributed scientific guidance and interpretation. AJI supervised the project, contributed to the methodology, tested the software, and provided feedback on its development. All authors reviewed, provided critical feedback, and edited the manuscript.

https://doi.org/10.5194/essd-2026-651
Preprint. Discussion started: 25 August 2026

Open Access Earth System Science Data Discussions

Acknowledgments

We thank the scientists and crew of research vessels at the Bedford Institute of Oceanography (Department of Fisheries and Oceans, Dartmouth, Nova Scotia, Canada) for their decades of work to collect this data and in particular Dr. Trevor Platt, Brian Irwin, Chantelle Layton, and Tim Perry for their relentless effort in collecting this unique dataset. Sadra Dehghani assisted with some of the data digitization. Financial support was provided by the Simons Foundation (award 595935 to AJI and 986772 to ZVF).

https://doi.org/10.5194/essd-2026-651
Preprint. Discussion started: 25 August 2026

Open Access Earth System Science Data Discussions

Table 1: Overview of the cruises and time series reports documenting photosynthesis–irradiance (PI) data compiled from 1973–2022. For each report (citation), the table lists the database code (Code), sampling years (Years), the incubator light source (Light), number of individual PI incubations (N), sampled depth range, incubation duration in hours (Duration), photosynthetically active radiation (PAR: available ✓ & missing ×), the proportion of light-saturated (LS), photoinhibited (Ph), and light-limited (LL) PI curves within each report, and the Longhurst biogeochemical provinces (Table. 2) for the sampling locations. Light source abbreviations are F = 150 W floodlight, H = 2000 W tungsten–halogen lamp, H* = 250 W tungsten–halogen lamp, and HR = 50 W Halogen Reflector.

Ref.	Code	Year	Light source	#NO.	Depth m	Duration h	PAR Wm^{-2}	Data Type (%) LS	Ph	LL	Longhurst Province
Irwin et al. (1975)	bb_mb_ch7375	1973-1975	F	183	0-10	4	×	0.68	0.32	0	NWCS
Cote and Platt (1984)	bb75	1975	F	69	5	3	✓	0.77	0.23	0	NWCS
Irwin and Platt (1978a)	bb7576	1975-1976	F	125	5	4	×	0.88	0.12	0	NWCS
Denma et al. (1977)	sh76	1976	F	94	0–50	3	×	0.77	0.23	0	GFST, NWCS
Irwin et al. (1978d)	baff77	1977	F	20	10-30	4	✓	0.45	0.55	0	BPLR
Irwin and Platt (1978b	bb77	1977	F	22	5	4	×	0.82	0.18	0	NWCS
Irwin et al. (1978a)	lab77	1977	F	32	10-30	4	✓	0.62	0.38	0	ARCT, BPLR
Irwin et al. (1978c	sh77	1977	F	34	10-30	3	✓	0.76	0.24	0	NWCS
Irwin et al. (1978b)	lab78	1978	F	32	10-30	4	✓	0.88	0.12	0	ARCT, BPLR, NWCS
Irwin et al. (1980)	scin78	1978	H	36	0-66	4	✓	0.06	0.94	0	ARCT, BPLR, NWCS
Irwin and Platt (1979)	sh78	1978	F	13	0-40	3	×	0.77	0.23	0	NWCS
Irwin et al. (1983d	sb78	1978-1979	H*	105	5-25	4	×	0.16	0.84	0	NWCS
Irwin et al. (1984)	lsl79	1979	H	96	0-10	4	×	0.49	0.51	0	ARCT, BERS, BPLR, NWCS, PSAE
Irwin et al. (1983e	sh79	1979	H	58	5-60	2-4	✓	0.05	0.95	0	GFST, NWCS
Irwin et al. (1982)	ung79	1979	H	97	5-43	0.5-4	×	0.53	0.47	0	BPLR
Irwin et al. (1983b	arc80	1980	H	126	1-64	2	✓	0.06	0.94	0	ARCT, BPLR, NWCS
Devred (2026)	bb80	1980	H*	64	5-50	0.5-4	×	0.23	0.77	0	NWCS
Irwin et al. (1983a	dis81	1981	H	86	3-150	3	×	0.04	0.95	0.01	NASE, NASW
Irwin et al. (1983c)	fb81	1981	H	21	0-40	3	×	0	1	0	BPLR
Irwin et al. (1983f	az82	1981-1982	H	44	0-88	4	✓	0.05	0.95	0	GFST, NASW, NWCS

Continued on next page

https://doi.org/10.5194/essd-2026-651
Preprint. Discussion started: 25 August 2026

Open Access Earth System Science Data Discussions

Table 1: Overview of the cruises and time series reports documenting photosynthesis–irradiance (PI) data compiled from 1973–2022. For each report (citation), the table lists the database code (Code), sampling years (Years), the incubator light source (Light), number of individual PI incubations (N), sampled depth range, incubation duration in hours (Duration), photosynthetically active radiation (PAR: available ✓ & missing ×), the proportion of light-saturated (LS), photoinhibited (Ph), and light-limited (LL) PI curves within each report, and the Longhurst biogeochemical provinces (Table. 2) for the sampling locations. Light source abbreviations are F = 150 W floodlight, H = 2000 W tungsten–halogen lamp, H* = 250 W tungsten–halogen lamp, and HR = 50 W Halogen Reflector.

Ref.	Code	Year	Light source	#NO.	Depth m	Duration h	PAR Wm^{-2}	Data Type (%) LS	Ph	LL	Longhurst Province
Irwin et al. (1988c)	hb82	1982	H	54	10-60	3	×	0.31	0.69	0	ARCT, BPLR, NWCS
Forbes et al. (1983)	bc85	1982-1983	H	85	0-30	1-2	×	0.48	0.52	0	ALSK, CCAL, NPTG
Irwin et al. (1986d)	arc83	1983	H	94	0-60	4	✓	0.14	0.86	0	ARCT, BPLR, NWCS
Irwin et al. (1985)	bda83	1983	H	31	10-80	2-4	✓	0.1	0.9	0	NASW, NWCS
Irwin et al. (1987b)	barb84	1984	H*	48	5-90	3	✓	0.12	0.88	0	CARB, NASW, NATR, NWCS
Irwin et al. (1986c	gb84	1984	H*	11	5-55	3	✓	0.55	0.45	0	NWCS
Irwin et al. (1987c)	js84	1984	H*	47	0-84	4	✓	0.15	0.85	0	BPLR
Irwin et al. (1986b	ls84	1984	H*	30	0-60	2-3	✓	0.23	0.77	0	ARCT, BPLR
Irwin et al. (1986a)	ls84_ia	1984	H*	25	0-25	3-4	×	0.76	0.24	0	BPLR, NWCS
Irwin et al. (1988a	bb85	1985	H*	63	1-15	3	×	0.48	0.52	0	NWCS
Irwin et al. (1988d)	gb85	1985	H*	25	1-80	3	×	0.36	0.64	0	GFST, NWCS
Irwin et al. (1987a	gbss85	1985	H*	160	5-130	3	✓	0.35	0.59	0.06	GFST, NASW, NWCS
Irwin et al. (1989b)	ls85	1985	H*	47	1-50	2-3	✓	0.26	0.74	0	ARCT, BPLR
Irwin et al. (1988b	cd86	1986	H*	90	5-80	3-4	×	0.23	0.77	0	NECS
Irwin et al. (1989a)	plasma87	1987	H*	48	5-110	3	×	0.12	0.88	0	GFST, NASW, NWCS
Irwin et al. (1990b	gb88	1988	H*	81	1-25	2	×	0.62	0.38	0	NWCS
Irwin et al. (1990c)	ls88	1988	H*	30	1-50	3	×	0.3	0.7	0	BPLR, NWCS
Irwin et al. (1990a	ss88	1988	H*	27	1-110	3	×	0.33	0.67	0	GFST, NASW, NWCS
Devred (2026)	unpublished	1989-2022	H* & HR	1398	0-100	NA, 3	×	0.58	0.42	0	ARAB, ARCT, BPLR, CARB, CNRY, GFST, MONS, NADR, NASE, NASW, NATR, NWCS, REDS

https://doi.org/10.5194/essd-2026-651
Preprint. Discussion started: 25 August 2026

Open Access Earth System Science Data Discussions

Table 2: Distribution of photosynthesis–irradiance (PI) incubations across Longhurst biogeochemical provinces in the compiled database. The table lists the Longhurst province code, corresponding biogeographical domain and province name, and the total number of individual PI observations (#) from each province. The dataset is dominated by observations from the Northwest Atlantic Shelves Province (NWCS) and the Boreal Polar Province (BPLR), with additional coverage spanning polar, coastal, westerlies, and tropical oceanic regions.

Province Code	**Domain – Longhurst Province Name**	**#**
NWCS	Coastal – NW Atlantic Shelves Province	1362
BPLR	Polar – Boreal Polar Province (POLR)	848
NASW	Westerlies – N. Atlantic Subtropical Gyral Province (West) (STGW)	422
ARCT	Polar – Atlantic Arctic Province	361
GFST	Westerlies – Gulf Stream Province	163
NASE	Westerlies – N. Atlantic Subtropical Gyral Province (East) (STGE)	128
NATR	Trades – N. Atlantic Tropical Gyral Province (TRPG)	117
NECS	Coastal – NE Atlantic Shelves Province	90
NADR	Westerlies – N. Atlantic Drift Province (WWDR)	64
ARAB	Coastal – NW Arabian Upwelling Province	56
CCAL	Coastal – California Upwelling Coastal Province	48
ALSK	Coastal – Alaska Downwelling Coastal Province	36
CARB	Trades – Caribbean Province	20
CNRY	Coastal – Canary Coastal Province (EACB)	18
REDS	Coastal – Red Sea, Persian Gulf Province	8
MONS	Trades – Indian Monsoon Gyres Province	4
BERS	Polar – N. Pacific Epicontinental Province	3
PSAE	Westerlies – Pacific Subarctic Gyres Province (East)	2
NPTG	Trades – N. Pacific Tropical Gyre Province	1

https://doi.org/10.5194/essd-2026-651
Preprint. Discussion started: 25 August 2026

Open Access Earth System Science Data Discussions

Table 3: Established commonly used photoinhibition models formulated with the parameters P_s, I^s_α, I^s_β and a positive shape parameter γ where $I^s_\alpha = P_s/\alpha$ and $I^s_\beta = P_s/\beta$. In the models, $P_{\max}$ was replaced with P_s as this factor does not represent the photosynthetic capacity; irradiance parameters have an s superscript since they are defined using P_s instead of $P_{\max}$, and $P_{\max}$ must be computed from P_s as shown in the right column. All models were fit with a constant intercept, R, which was omitted from the table.

Name & Authors	**Equation**	**Photosynthetic Capacity, $P_{\max}$**
Established 4 parameter models		
Ph02: Peeters & Eilers, 1978 Peeters and Eilers (1978)	$P_s(I/I^s_\alpha)\left(1+\frac{I}{I^s_\alpha}+\frac{I^2}{I^s_\alpha I^s_\beta}\right)^{-1}$	$\frac{P_s}{1+2\sqrt{\beta/\alpha}}$
Ph03: Platt et al., 1980 Platt et al. (1980)	$P_s\left(1-e^{-I/I^s_\alpha}\right)e^{-I/I^s_\beta}$	$P_s\left(\frac{\alpha}{\alpha+\beta}\right)\left(\frac{\beta}{\alpha+\beta}\right)^{\beta/\alpha}$
Ph04: Neale & Richerson, 1987 Neale and Richerson (1987)	$P_s\tanh\left(\frac{I}{I^s_\alpha}\right)e^{-I/I^s_\beta}$	$P_s\tanh\left(\frac{I_{\text{sat}}}{I^s_\alpha}\right)\exp\left(-\frac{I_{\text{sat}}}{I^s_\beta}\right)$
Ph05: Baly, 1935 Baly (1935)	$P_s\left(\frac{I}{I+I^s_\alpha}\right)e^{-I/I^s_\beta}$	$P_s\left(\frac{I_{\text{sat}}}{I_{\text{sat}}+I^s_\alpha}\right)\exp\left(-\frac{I_{\text{sat}}}{I^s_\beta}\right)$
Ph06: Smith, 1936 Amirian-matlob (2025)	$P_s\left(\frac{I}{\sqrt{I^2+(I^s_\alpha)^2}}\right)e^{-I/I^s_\beta}$	$P_s\left(\frac{I_{\text{sat}}}{\sqrt{I^2_{\text{sat}}+(I^s_\alpha)^2}}\right)\exp\left(-\frac{I_{\text{sat}}}{I^s_\beta}\right)$
Established 5 parameter models		
Ph07: Bannister, 1979 Bannister (1979)	$P_s I\left(I^\gamma+I^\gamma_\alpha\right)^{-1/\gamma}e^{-I/I^s_\beta}$	Numerical

* Saturation irradiance, I_{sat} can be derived from equations $\frac{P_s}{2\alpha}\left(2\alpha\beta^{-1}+\sqrt{(2\alpha\beta^{-1})^2+1}\right)$ for Ph04, $\frac{P_s}{2\alpha}\left(\sqrt{1+4\alpha\beta^{-1}}-1\right)$ for Ph05, and from the numerical solution of the equation $I^3_{\text{sat}}+(P_s\alpha^{-1})^2 I_{\text{sat}}-(P_s\alpha^{-1})^2(P_s\beta^{-1})=0$ for Ph06.

Table 4: Mean differences (± SD) in photosynthetic parameters between community and size-fractionated samples. An asterisk (*) denotes that the corresponding 95% confidence interval does not include zero and also $I_\alpha = P_{\max}/\alpha$ and $I_\beta = P_{\max}/\beta$.

Size fraction	Code	n	$P_{\max}$	α	β	I_α	I_β
<1 μm	az82	4	0.41 ± 0.36	0.67 ± 0.40	0.66 ± 0.48	-0.19 ± 0.06*	-0.23 ± 0.14
	ls85	4	-0.18 ± 0.42	-0.09 ± 0.27	-0.40 ± 0.18*	-0.12 ± 0.52	0.36 ± 0.49
	gbss85	7	-0.24 ± 0.09*	0.12 ± 0.12	-0.25 ± 0.14	-0.25 ± 0.12*	-0.01 ± 0.08
	bda83	8	-0.41 ± 0.15*	0.36 ± 0.57	-0.27 ± 0.14*	-0.52 ± 0.03*	-0.16 ± 0.07*
	arc83	11	-0.51 ± 0.21*	-0.18 ± 0.30	-0.37 ± 0.22	-0.35 ± 0.09*	-0.18 ± 0.09*
	cd86	11	-0.41 ± 0.09*	-0.30 ± 0.11*	-0.47 ± 0.09*	-0.22 ± 0.08*	0.05 ± 0.05
<3 μm	cd86	3	-0.13 ± 0.02*	0.00 ± 0.02	-0.02 ± 0.10	-0.13 ± 0.02*	-0.10 ± 0.09
<5 μm	cd86	3	0.04 ± 0.05	0.20 ± 0.07*	-0.14 ± 0.05*	-0.14 ± 0.02*	0.20 ± 0.07*
>1 μm	az82	3	0.06 ± 0.32	-0.02 ± 0.25	-0.27 ± 0.22	0.14 ± 0.11	0.45 ± 0.02*
	ls85	4	-0.07 ± 0.11	-0.07 ± 0.21	-0.05 ± 0.29	0.03 ± 0.14	0.16 ± 0.49
	bda83	7	0.18 ± 0.20	-0.05 ± 0.18	0.19 ± 0.16	0.22 ± 0.06*	0.02 ± 0.03
	gbss85	9	0.10 ± 0.34	-0.10 ± 0.32	-0.14 ± 0.35	0.27 ± 0.08*	0.32 ± 0.19
	arc83	13	-0.16 ± 0.17	-0.16 ± 0.15	-0.14 ± 0.12	0.08 ± 0.12	-0.05 ± 0.07
	cd86	17	-0.04 ± 0.05	-0.13 ± 0.06*	-0.16 ± 0.04*	0.04 ± 0.04	0.11 ± 0.06
	dis81	18	0.44 ± 0.13*	0.10 ± 0.20	0.82 ± 0.40*	0.20 ± 0.16	-0.10 ± 0.22

https://doi.org/10.5194/essd-2026-651
Preprint. Discussion started: 25 August 2026

Open Access Earth System Science Data Discussions

Table 5: Correction factors used to transform parameter estimates from commonly used PI models (Table 3) to the equivalent parameters of the double-tanh model (Eq. 1). Each row corresponds to one of the commonly used PI models, denoted Ph02–Ph07 following the notation implemented in `piCurve::Model_piCurve()` Amirian and Irwin (2025). Separate regression models were fitted for each double-tanh parameter with the corresponding model parameters used as predictors. All estimated regression coefficients were statistically significant.

double-tanh parameter	**Model**	**Intercept**	**Slope**		
			α	β	P_s
α		-1.37	0.71	—	—
β	**Ph02**: Peeters and Eilers (1978)	-4.97	0.31	0.04	0.62
$P_{\max}$		-0.42	—	—	1.00
α		-0.74	0.85	—	—
β	**Ph03**: Platt et al. (1980)	-4.83	0.30	0.02	0.62
$P_{\max}$		-0.22	—	—	1.00
α		-0.36	0.87	—	—
β	**Ph04**: Neale and Richerson (1987)	-4.40	0.33	0.06	0.55
$P_{\max}$		-0.18	—	—	0.99
α		-1.55	0.64	—	—
β	**Ph05**: Baly (1935)	-5.12	0.24	0.04	0.62
$P_{\max}$		-0.44	—	—	1.00
α		-0.40	0.88	—	—
β	**Ph06**: Smith (1936)	-4.46	0.30	0.08	0.57
$P_{\max}$		-0.24	—	—	0.98
α		-1.44	0.61	—	—
β	**Ph07**: Bannister (1979)	-4.94	0.20	0.07	0.64
$P_{\max}$		-0.41	—	—	1.09

https://doi.org/10.5194/essd-2026-651
Preprint. Discussion started: 25 August 2026

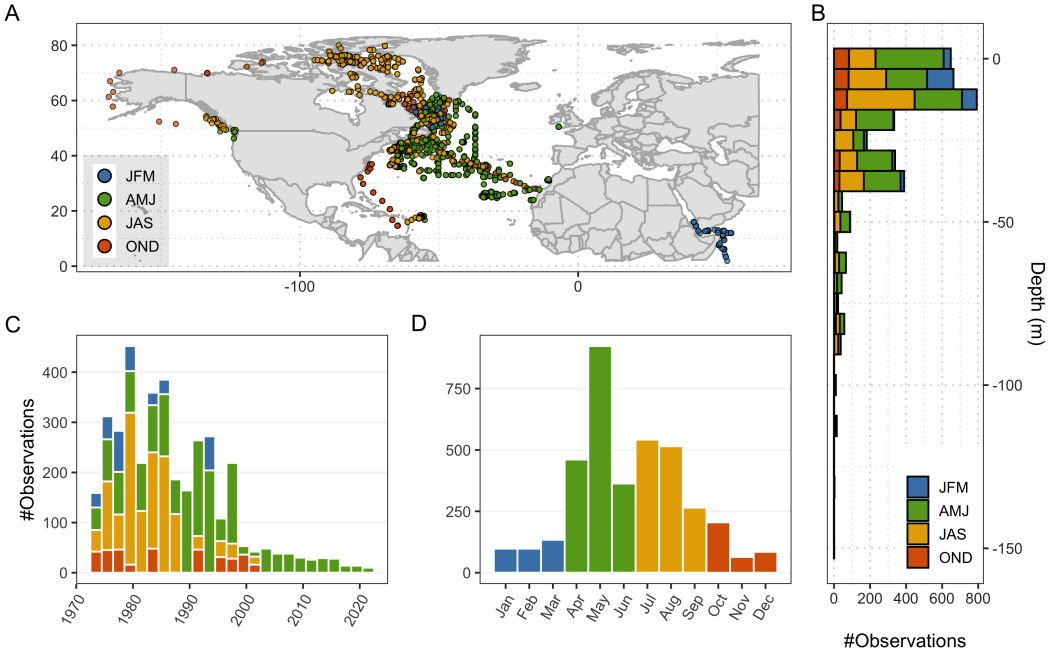

Figure 1: Spatial and temporal distribution of ^{14}C PI incubations. (A) Location of 3,751 BIO PI incubation experiments (1973–2022) from 822 oceanographic stations taken from sea surface to 150 m color coded by seasons (JFM, AMJ, JAS, OND). Histograms illustrate (B) the sampling depth for each PI curve as well as the distribution of sampling by (C) year and (D) month, highlighting the seasonal peak during May and the dominance of data collected prior to 2000.

https://doi.org/10.5194/essd-2026-651
Preprint. Discussion started: 25 August 2026

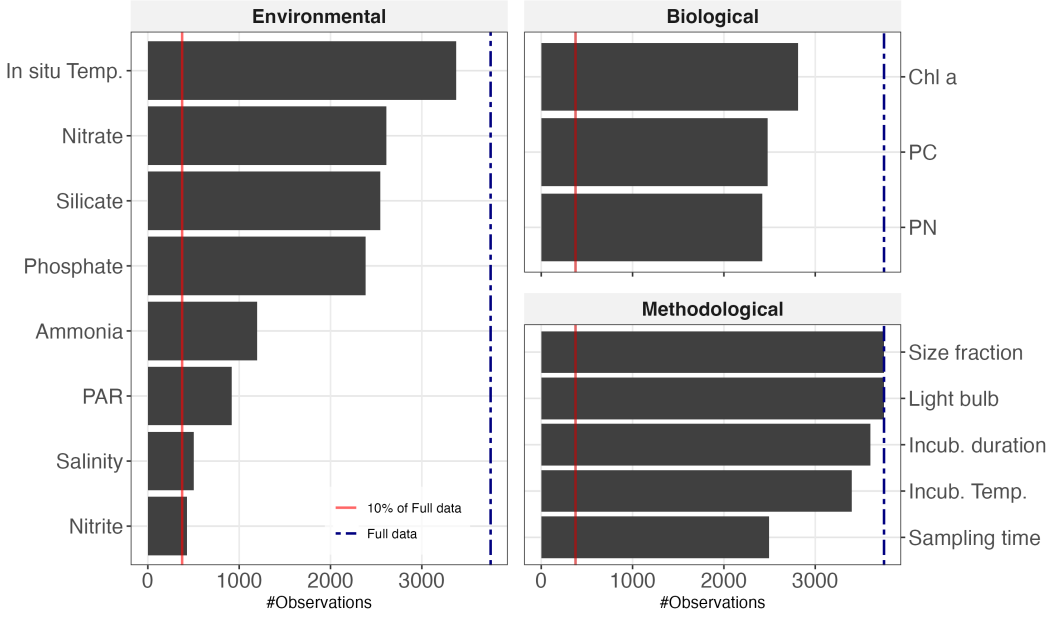

Figure 2: Frequency of observation of ancillary variables for each PI curve. Each PI curve has an associated sampling date (year, month, and day) and location (latitude, longitude, depth). Bar plots show the number of observations for additional variables grouped by category: (A) Methodological, (B) Biological, and (C) Environmental. The navy blue dashed line marks the total number of samples (n = 3,751) and the solid line marks 10% of total data samples, as shown in the legend. Chlorophyll-*a* concentration was used to normalize photosynthetic rate but was not reported separately for about one-quarter of the PI curves.

https://doi.org/10.5194/essd-2026-651
Preprint. Discussion started: 25 August 2026

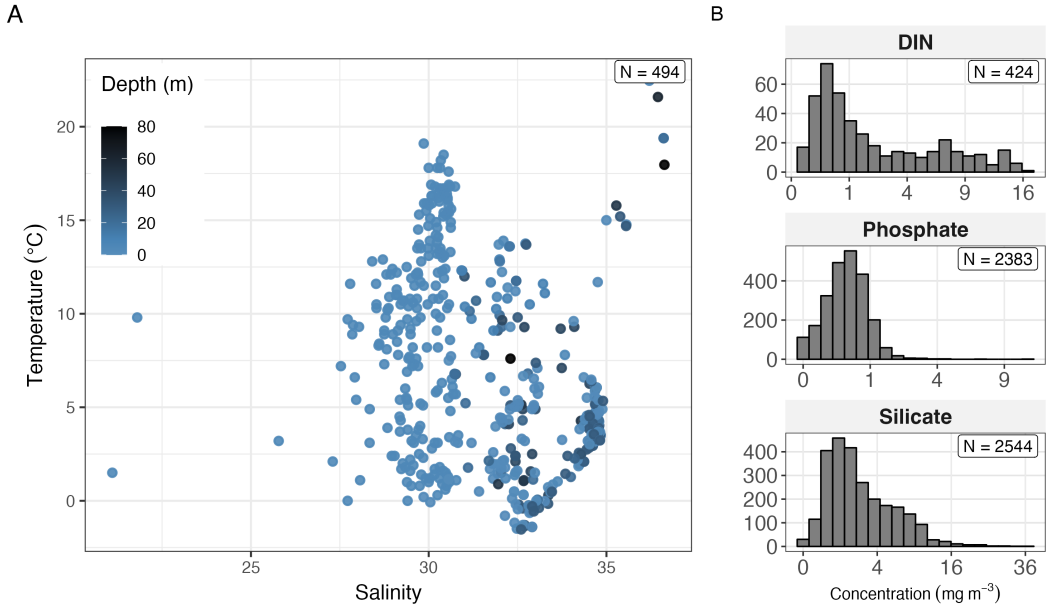

Figure 3: Distribution of environmental and chemical data across PI curves. (A) T-S diagram coloured by sampling depth (N = 494, scatterplot of temperature vs. salinity). (B) Histograms of total nitrogen concentration, DIN (mg m^{-3}, = nitrate + nitrite + ammonia, N = 424), phosphate concentration (mg m^{-3}, N = 2383) and silicate concentration (mg m^{-3}, N = 2544) on a square root axis.

https://doi.org/10.5194/essd-2026-651
Preprint. Discussion started: 25 August 2026

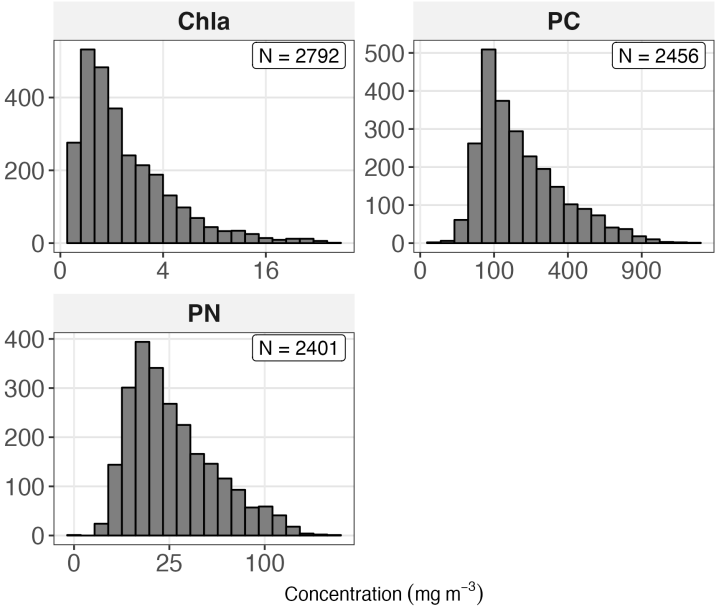

Figure 4: Frequency distributions of chlorophyll-*a* (Chla), particulate organic carbon (POC), and particulate nitrogen (PON) concentrations associated with PI experiments. Histograms are shown using square-root transformed concentrations to improve visualization of the positively skewed distributions, while axis labels are presented on the original concentration scale (mg m^{-3}). Sample sizes for each variable are indicated within panels. Twenty-two ice-associated samples with exceptionally large concentrations (e.g., PC up to 10,847 mg m^{-3}, PN up to 1,426 mg m^{-3}, and Chla up to 191 mg m^{-3} were excluded from the visualization to prevent compression of the dominant open-water distributions.

https://doi.org/10.5194/essd-2026-651
Preprint. Discussion started: 25 August 2026

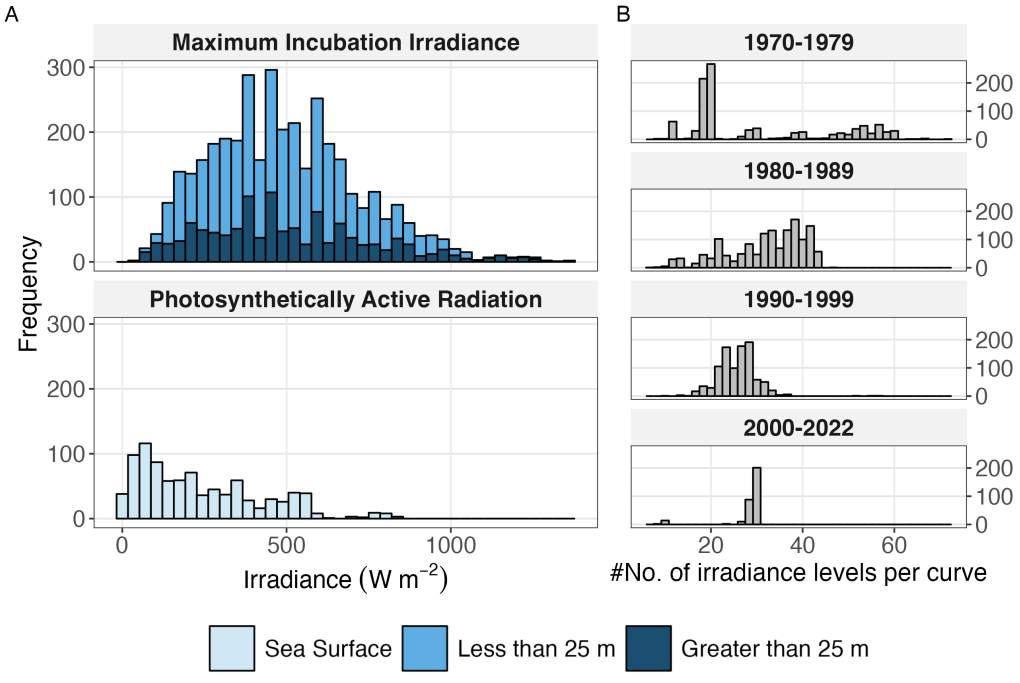

Figure 5: Number and range of treatment irradiances for each PI curve compared to sea-surface PAR. (A) Histogram showing (top panel) the maximum irradiance (W m^{-2}) for each PI curve, coloured according to the sample depth; (bottom panel) Sea surface photosynthetically active radiation (PAR) measured at the time sample taken (PAR is missing for 2/3 of the cases). (B) Histogram showing how the distribution of the number of discrete irradiances for each PI curve changed over decades.

https://doi.org/10.5194/essd-2026-651
Preprint. Discussion started: 25 August 2026

Open Access Earth System Science Data Discussions

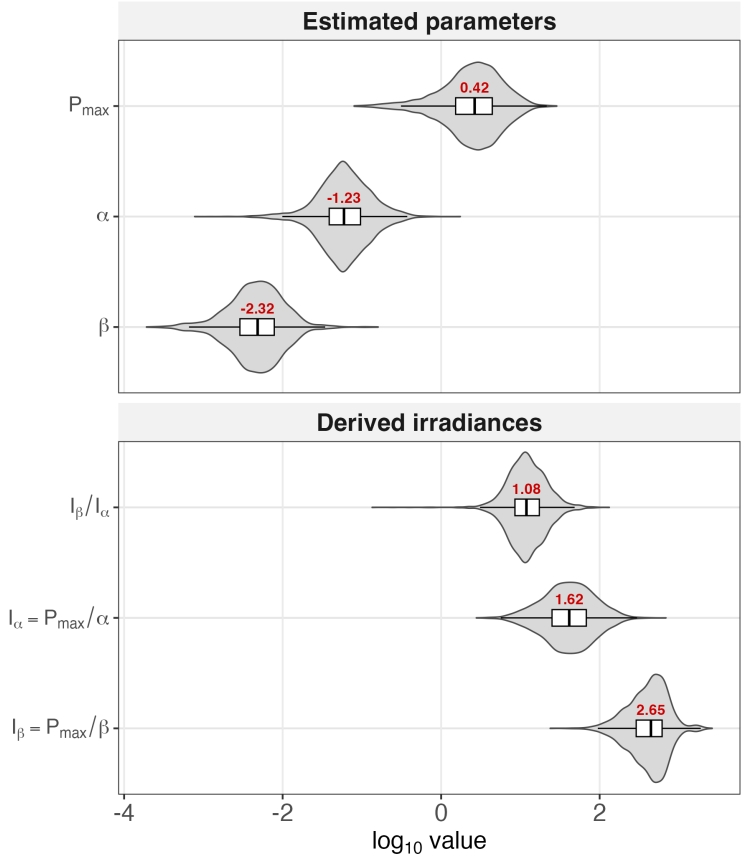

Figure 6: Distribution of estimated PI parameters and derived irradiance metrics across all fitted PI curves. Violin plots show the distributions of the maximum photosynthetic rate ($P_{\max}$), photosynthetic efficiency (α), photoinhibition rate (β), light-saturation irradiance $I_\alpha = P_{\max}/\alpha$, photoinhibition onset irradiance $I_\beta = P_{\max}/\beta$, and their ratio I_β/I_α on a $\log_{10}$ scale. Boxplots embedded within each violin indicate the median, shown in red, and interquartile range. The separation between I_α and I_β demonstrates that photoinhibition generally occurs at irradiances substantially higher than those required for light saturation.

https://doi.org/10.5194/essd-2026-651
Preprint. Discussion started: 25 August 2026

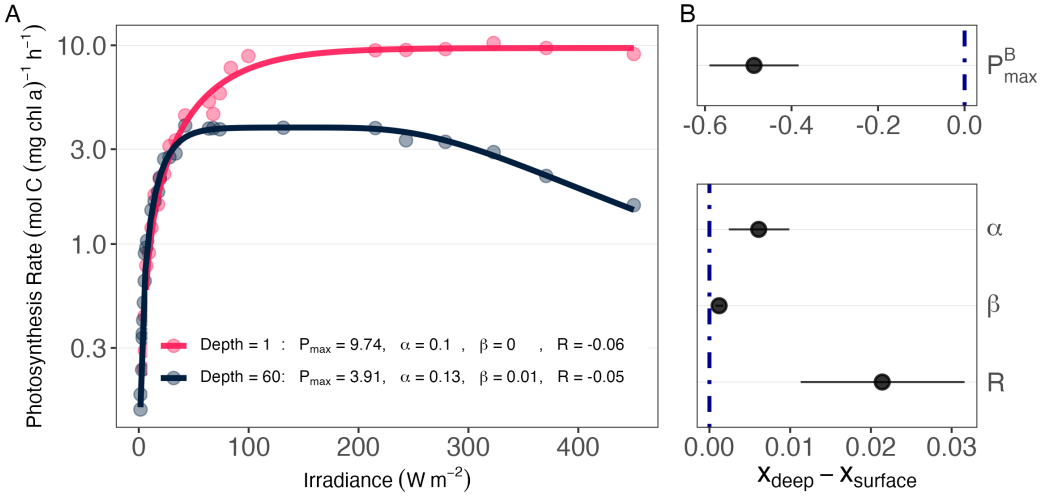

Figure 7: Depth-dependent differences in PI parameters. (A) display of two PI experiments taken from the same location but different depth (1 and 60 m) along with their fitted model and associated estimated PI parameters, summarized in the legend ($R^2 \geq 0.98$). (B) Pairwise t-test comparisons of PI curve parameters down the water column. Solid points indicate the mean difference between parameter estimates from paired shallow and deep samples collected at the same location. Error bars denote 95% confidence intervals. For each parameter, X_{deep} refers to the estimate from the deeper sample, and $X_{surface}$ to its corresponding shallow counterpart . Units for P^B_{max} and R is mg C (mg chl a)$^{-1}$ h^{-1} and for α and β is mg C (mg chl a)$^{-1}$ h^{-1} m^2 W^{-1}.

https://doi.org/10.5194/essd-2026-651
Preprint. Discussion started: 25 August 2026

Open Access Earth System Science Data Discussions

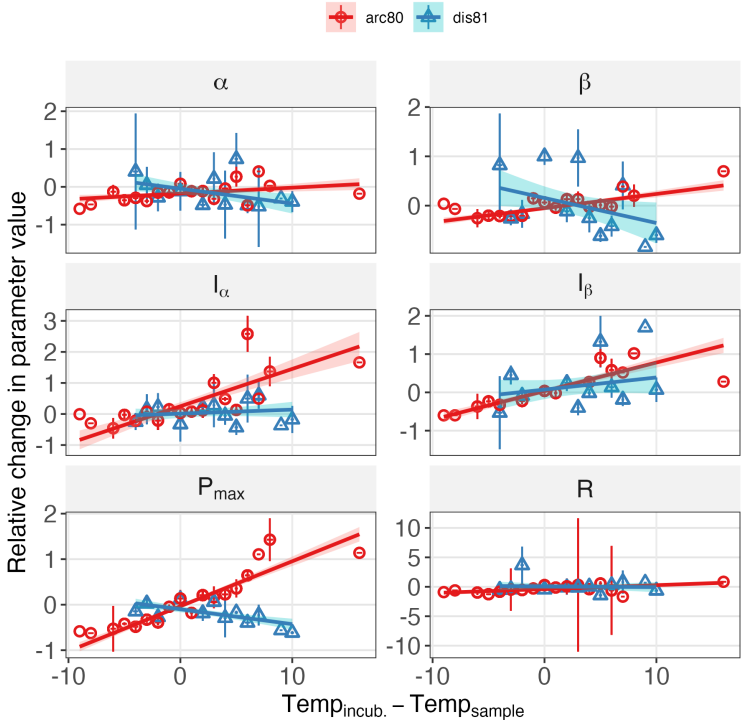

Figure 8: Effect on PI parameters of changing incubation temperature compared to *in situ* temperature. Relative differences in PI parameters (P_{max}, α, β, R) and the derived irradiance metrics I_α and I_β as a function of the temperature difference between incubation and in situ sample temperature (ΔT = $\text{Temp}_{\text{incub}}$ − $\text{Temp}_{\text{sample}}$). Each point represents the mean relative difference over a set of experiments with temperature offset rounded to the nearest 1°C, with error bars showing the standard error of the relative differences. Data from two cruises (`arc80` and `dis81`) with average in situ temperature of 3.43°C and 18.4°C, respectively. Linear regressions (±95% confidence interval shading) summarize the temperature response for each dataset (`arc80` and `dis81`). No other cruises had temperature manipulation experiments.

https://doi.org/10.5194/essd-2026-651
Preprint. Discussion started: 25 August 2026

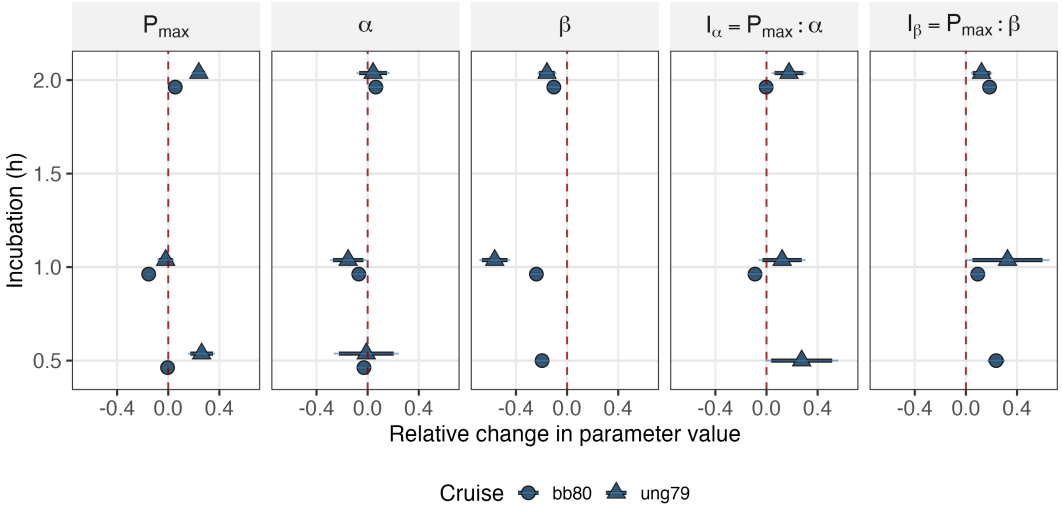

Figure 9: Effects of incubation duration on PI parameters relative to a reference incubation time of 4 h. Relative differences in PI parameters ($P_{\max}$, α, β) and the derived irradiance metrics I_α and I_β as a function of incubation duration. Points indicate group-level mean differences, with horizontal bars denoting 95% (blue) and 90% (black) confidence intervals derived from multivariate meta-analysis that accounts for parameter uncertainty and inter-parameter covariance. The vertical dashed line indicates no difference relative to the 4 h incubation baseline. Negative relative changes indicate lower values observed in PI parameters relative to the reference incubation time of 4 h, whereas positive relative changes indicate higher values. The largest sample size is 73 for `ung79` with a 2-hour incubation, while sample sizes for all other cases range between 4 and 7.

https://doi.org/10.5194/essd-2026-651
Preprint. Discussion started: 25 August 2026

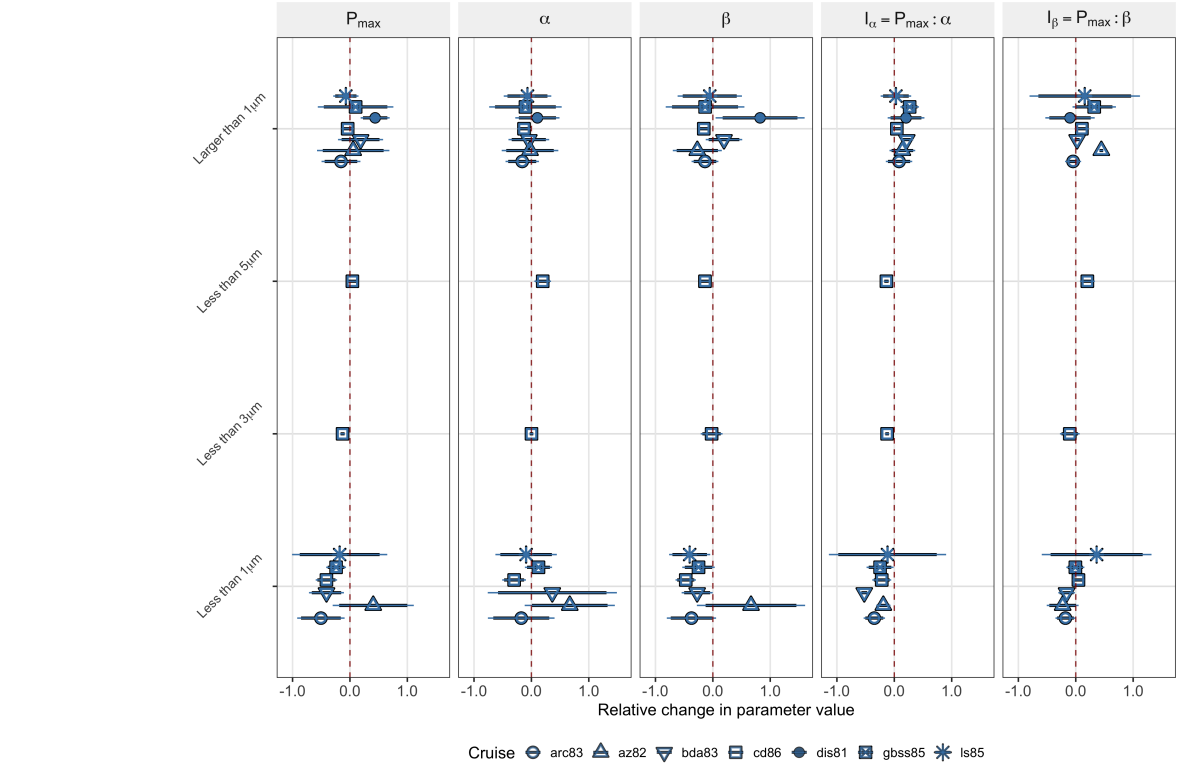

Figure 10: Variation in PI parameters across selected size fractions compared to whole community (bulk) samples. Relative differences in PI parameters ($P_{\max}$, α, β) and the derived irradiance metrics I_α and I_β as a function of size fractionations (less than 1, 3, 5 μm & larger than 5 μm). Each point represents the median relative difference for a given cruise and size class relative to data from whole community samples, with vertical bars indicating 95% (blue) and 90% (black) bootstrap confidence intervals (10,000 resamples). value < 0 indicates lower values in the size fraction relative to the community sample, whereas value > 0 indicates higher values. Quantitative summaries of median ratios and median absolute deviations along with sample sizes are provided in Table. 4.

https://doi.org/10.5194/essd-2026-651
Preprint. Discussion started: 25 August 2026

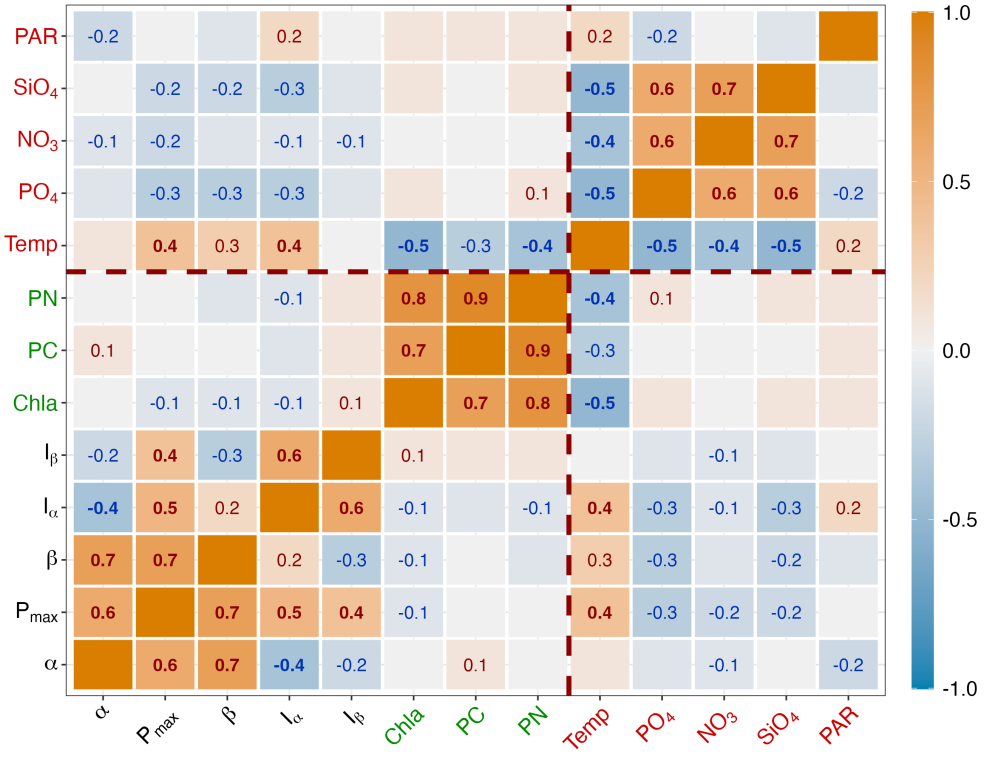

Figure 11: Correlation structure of photosynthesis–irradiance parameters with cellular and environmental variables. Heat maps show Pearson correlation coefficients among PI parameters ($P_{\max}$, α, β), photoacclimation irradiances (I_α and I_β), cellular properties (Chl*a*, PC, and PN), and environmental variables (temperature, NO_3^-, PO_4^{3-}, SiO_4). Correlations are computed on log–log–transformed variables using `Hmisc::rcorr`. Only statistically significant correlations ($p < 0.001$) are displayed; blank cells indicate non-significant relationships. Color denotes correlation magnitude and sign. Upper and lower triangles show identical information for visual clarity.

https://doi.org/10.5194/essd-2026-651
Preprint. Discussion started: 25 August 2026

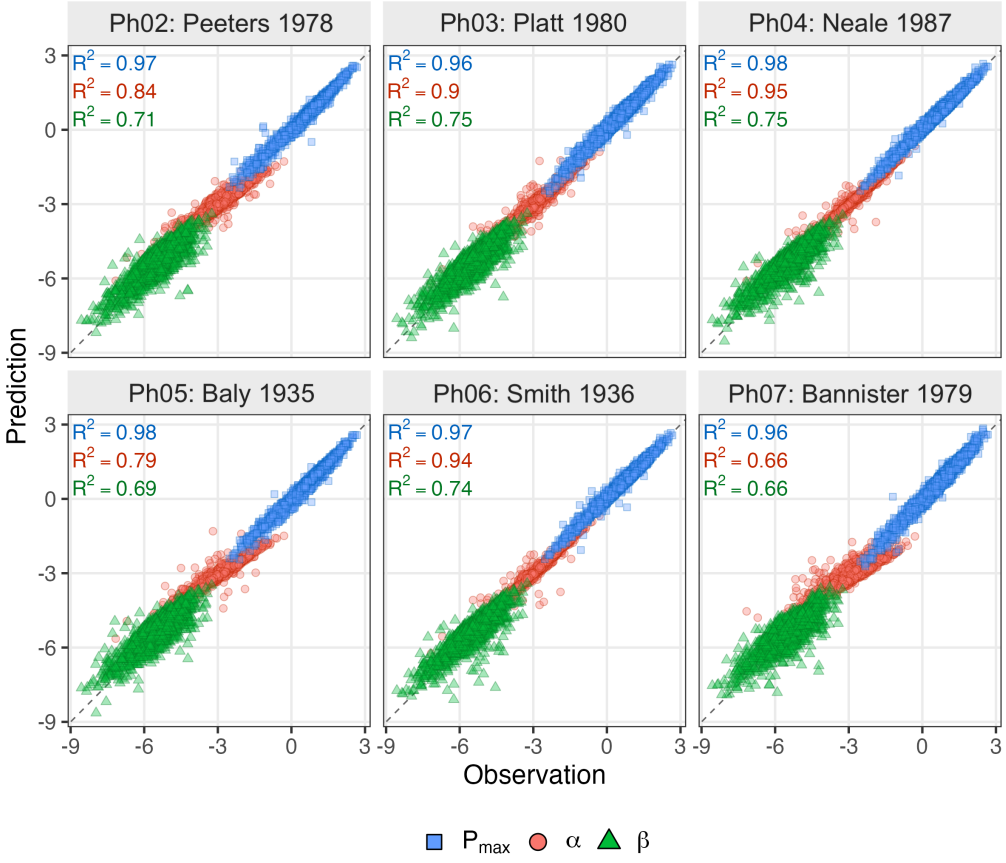

Figure 12: Comparison of observed and predicted parameter values for photoinhibition models used in our study. Predicted values obtained from linear regressions are plotted against observed values of reference double-tanh model (Eq. 1) for the three key PI parameters: maximum photosynthetic rate ($P_{\max}$, blue squares), photosynthetic efficiency (α, red circles), and photoinhibition rate (β, green triangles). All variables are shown on the natural logarithmic scale. The dashed line denotes the 1:1 relationship, with points lying closer to the line indicating better agreement between predicted and observed values. Corresponding coefficients of determination (R^2) for $P_{\max}$, α, and β are reported within each panel. Overall, the regressions reproduced $P_{\max}$ most accurately ($R^2 = 0.96$–0.98), followed by α ($R^2 = 0.66$–0.95), whereas β exhibited the greatest variability ($R^2 = 0.66$-0.75). Estimated regression coefficients and associated statistics are provided in Table. 5, and the panels are named by authors' name followed by year.

https://doi.org/10.5194/essd-2026-651
Preprint. Discussion started: 25 August 2026

Open Access Earth System Science Data Discussions

References

Amirian, M. M. and Irwin, A. J.: PiCurve: an R package for modeling photosynthesis-irradiance curves, arXiv preprint arXiv:2508.14321, 2025.

Amirian, M. M., Irwin, A. J., and Finkel, Z. V.: Extending the Monod model of microbal growth with memory, Frontiers in Marine Science, 9, 963 734, 2022.

Amirian, M. M., Finkel, Z. V., Devred, E., and Irwin, A. J.: Parameterization of Photoinhibition for Phytoplankton, Zenodo, https://doi.org/10.5281/zenodo.16748102, 2025a.

Amirian, M. M., Finkel, Z. V., Devred, E., and J. Irwin, A.: Parameterization of photoinhibition for phytoplankton, Communications Earth & Environment, 6, 707, 2025b.

Amirian, M. M., Devred, E., Clay, S., Finkel, Z. V., and Irwin, A. J.: A Compilation of Marine Photosynthesis–Irradiance Data from ^{14}C Incubation Experiments, Zenodo, https://doi.org/10.5281/zenodo.21908199, 2026.

Amirianmatlob, M.: Modelling Phytoplankton Growth Rates Under Changing Resource Conditions, Ph.D. thesis, Dalhousie, 2025.

Baly, E. C. C.: The kinetics of photosynthesis, Proceedings of the Royal Society of London. Series B-Biological Sciences, 117, 218–239, 1935.

Bannister, T.: Quantitative description of steady state, nutrient-saturated algal growth, including adaptation, Limnology and Oceanography, 24, 76–96, 1979.

Becker, S., Aoyama, M., Woodward, E. M. S., Bakker, K., Coverly, S., Mahaffey, C., and Tanhua, T.: GO-SHIP repeat hydrography nutrient manual: the precise and accurate determination of dissolved inorganic nutrients in seawater, using continuous flow analysis methods, Frontiers in marine science, 7, 581 790, 2020.

Behrenfeld, M. J. and Falkowski, P. G.: Photosynthetic rates derived from satellite-based chlorophyll concentration, Limnology and oceanography, 42, 1–20, 1997.

Blackman, F. F.: Optima and limiting factors, Annals of botany, 19, 281–295, 1905.

Bouman, H. A., Platt, T., Doblin, M., Figueiras, F. G., Gudmundsson, K., Gudfinnsson, H. G., Huang, B., Hickman, A., Hiscock, M., Jackson, T., et al.: Photosynthesis–irradiance parameters of marine phytoplankton: synthesis of a global data set, Earth System Science Data, 10, 251–266, 2018.

Bricaud, A., Babin, M., Morel, A., and Claustre, H.: Variability in the chlorophyll-specific absorption coefficients of natural phytoplankton: Analysis and parameterization, Journal of Geophysical Research: Oceans, 100, 13 321–13 332, 1995.

Britten, G. L., Jönsson, B., Kulk, G., Bouman, H. A., Follows, M. J., and Sathyendranath, S.: Predicting photosynthesis–irradiance relationships from satellite remote-sensing observations, Limnology and Oceanography Letters, 10, 967–976, 2025.

Cote, B. and Platt, T.: Daily phytoplankton productivity experiments and nutrient measurements in Bedford Basin, Nova Scotia, from 18 May to 26 July 1975, Technical report 425, Canadian Data Report of Fisheries and Aquatic Sciences, 1984.

Croteau, D., Guérin, S., Savoie, M., Donaher, N., M. Amirian, M., Babin, M., Campbell, D. A., and Lavaud, J.: Nonphotochemical quenching and beyond: multi-layered photoprotection shapes light-stress tolerance across seasonal niches in Arctic diatoms, Frontiers in Photobiology, 3, 1745 893, 2025.

Denman, K., Irwin, B., and Platt, T.: Phytoplankton Productivity Experiments and Nutrient Measurements at the Edge of the Nova Scotia Continental Shelf Between June 28 and July 12, 1976, Technical report 708, Fisheries and Marine Service Technical Report, 1977.

Devred, E.: Database of photosynthesis–irradiance experiments, unpublished database, 2026.

https://doi.org/10.5194/essd-2026-651
Preprint. Discussion started: 25 August 2026

Devred, E., Clay, S., Ringuette, M., Perry, T., Amirian, M., Irwin, A., and Finkel, Z.: Net primary production in the Labrador Sea between 2014 and 2022 derived from ocean colour remote sensing based on ecological regimes, Remote Sensing of Environment, 323, 114 713, 2025.

DeVries, T.: The ocean carbon cycle, Annual Review of Environment and Resources, 47, 317–341, 2022.

Everett, J. D. and Doblin, M. A.: Characterising primary productivity measurements across a dynamic western boundary current region, Deep Sea Research Part I: Oceanographic Research Papers, 100, 105–116, 2015.

Fasham, M. J. R. and Platt, T.: Photosynthetic response of phytoplankton to light: a physiological model, Proceedings of the Royal society of London. Series B. Biological sciences, 219, 355–370, 1983.

Field, C. B., Behrenfeld, M. J., Randerson, J. T., and Falkowski, P.: Primary production of the biosphere: integrating terrestrial and oceanic components, science, 281, 237–240, 1998.

Finkel, Z. V.: Light absorption and size scaling of light-limited metabolism in marine diatoms, Limnology and oceanography, 46, 86–94, 2001.

Forbes, J. R., Sefton, H. A., and de Macedo: Phytoplankton productivity experiments in British Columbia coastal waters, 1982 and 1983, Technical report, Canadian Data Report of Fisheries and Aquatic Sciences, 1983.

Fragoso, G. M., Poulton, A. J., Yashayaev, I. M., Head, E. J., and Purdie, D. A.: Spring phytoplankton communities of the Labrador Sea (2005–2014): pigment signatures, photophysiology and elemental ratios, Biogeosciences, 14, 1235–1259, 2017.

Gallegos, C. L.: Phytoplankton photosynthetic capacity in a shallow estuary: environmental correlates and interannual variation, Marine Ecology Progress Series, 463, 23–37, 2012.

Gasol, J. M., Cardelús, C., Morán, X. A. G., Balagué, V., Forn, I., Marrasé, C., Massana, R., Pedrós-Alió, C., Sala, M. M., Simó, R., et al.: Seasonal patterns in phytoplankton photosynthetic parameters and primary production at a coastal NW Mediterranean site, Scientia Marina, 2016.

Gasparrini, A. and Armstrong, B.: Reducing and meta-analysing estimates from distributed lag non-linear models, BMC medical research methodology, 13, 1, 2013.

Gasparrini, A., Armstrong, B., and Kenward, M. G.: Multivariate meta-analysis for non-linear and other multi-parameter associations, Statistics in medicine, 31, 3821–3839, 2012.

Harrell Jr, F. E.: Package 'hmisc', CRAN2018, 2019, 235–236, 2019.

Holm-Hansen, O., Lorenzen, C. J., Holmes, R. W., and Strickland, J. D. H.: Fluorometric Determination of Chlorophyll, Journal du Conseil, 30, 3–15, 1965.

IPCC: Climate Change 2021: The Physical Science Basis. Contribution of Working Group I to the Sixth Assessment Report of the Intergovernmental Panel on Climate Change, Cambridge University Press, Cambridge, United Kingdom and New York, NY, USA, doi:10.1017/9781009157896, 2021.

Irwin, B. and Platt, T.: Phytoplankton productivity experiments and nutrient measurements in Bedford Basin, Nova Scotia, from September 1975 to December 1976, Technical report 762, Fisheries and Marine Service Technical Report, 1978a.

Irwin, B. and Platt, T.: Phytoplankton productivity experiments and nutrient measurements in Bedford Basin, Nova Scotia, from January 1977 to July 1977, Technical report 93, Fisheries and Marine Service Technical Report, 1978b.

Irwin, B. and Platt, T.: Phytoplankton Productivity and Nutrient Measurements at the Edge of the Continental Shelf off Nova Scotia between June 3 and June 6, 1978, Technical report 174, Canadian Data Report of Fisheries and Aquatic Sciences, 1979.

Irwin, B., Platt, T., Jassby, A. D., and Subba Rao, D. V.: The Relationship Between Light Intensity and Photosynthesis by Phytoplankton: Results of Experiments at Three Stations in the Coastal Waters of

https://doi.org/10.5194/essd-2026-651
Preprint. Discussion started: 25 August 2026

Nova Scotia, Technical report 595, Fisheries and Marine Service Research and Development Technical Report, 1975.

Irwin, B., Evans, P., and Platt, T.: Phytoplankton productivity experiments and nutrient measurements in the Labrador Sea from 15 October to 31 October 1977, Technical report 83, Fisheries and Marine Service Technical Report, 1978a.

Irwin, B., Evans, P., and Platt, T.: Phytoplankton productivity experiments and nutrient measurements in the Labrador Sea, from 11 February to 28 February 1978, Technical report 114, Fisheries and Marine Service Technical Report, 1978b.

Irwin, B., Harrison, W. G., Denman, K., and Platt, T.: Phytoplankton productivity and nutrient measurements at the edge of the continental shelf off Nova Scotia between April 28 and May 11, 1977, Technical report 62, Fisheries and Marine Service Technical Report, 1978c.

Irwin, B., Hodgson, M., Dickie, P., and Platt, T.: Phytoplankton productivity experiments in Baffin Bay and adjacent inlets from 22 August to 18 September 1977, Technical report 82, Fisheries and Marine Service Technical Report, 1978d.

Irwin, B., Harrison, W. G., Gallegos, C. L., and Platt, T.: Phytoplankton productivity experiments and nutrient measurements in the Labrador Sea, Davis Strait, Baffin Bay and Lancaster Sound from 26 August to 14 September 1978, Technical report 213, Canadian Data Report of Fisheries and Aquatic Sciences, 1980.

Irwin, B., Platt, T., Harrison, W. G., Gallegos, C. L., and Lindley, P.: Phytoplankton productivity experiments and nutrient measurements in Ungava Bay, N.W.T., from August 1 to September 3, 1979, Technical report 287, Canadian Data Report of Fisheries and Aquatic Sciences, 1982.

Irwin, B., Caverhill, C., Subba Rao, D. V., and Platt, T.: Primary productivity measurements in the chlorophyll maximum in the vicinity of the Mid-Atlantic Ridge, west of the Azores, from 8 July to 25 July, 1982, Technical report 402, Canadian Data Report of Fisheries and Aquatic Sciences, 1983a.

Irwin, B., Harris, L., Dickie, P., Lindley, P., and Platt, T.: Phytoplankton productivity in the Eastern Canadian Arctic during July and August 1980, Technical report 386, Canadian Data Report of Fisheries and Aquatic Sciences, 1983b.

Irwin, B., Harris, L., Hodgson, M., Horne, E., and Platt, T.: Primary Productivity and Nutrient Measurements in Northern Foxe Basin, N.W.T. from 27 August to 7 September 1981, Technical report 385, Canadian Data Report of Fisheries and Aquatic Sciences, 1983c.

Irwin, B., Harrison, W. G., and Platt, T.: Plankton dynamics in Bedford Basin, Nova Scotia: Phytoplankton productivity experiments and nutrient measurements from February 13, 1978 until March 14, 1979, Technical report 272, Canadian Data Report of Fisheries and Aquatic Sciences, 1983d.

Irwin, B., Lindley, P., Gallegos, C. L., and Platt, T.: Phytoplankton productivity experiments on the Scotian Shelf from April 18 to May 2, Technical report 384, Canadian Data Report of Fisheries and Aquatic Sciences, 1983e.

Irwin, B., Platt, T., Lindley, P., Fasham, M. J., and Jones, K.: Phytoplankton productivity in the vicinity of a front, S.W. of the Azores during May 1981, Technical report 400, Canadian Data Report of Fisheries and Aquatic Sciences, 1983f.

Irwin, B., Dickie, P., Lindley, P., and Platt, T.: Phytoplankton productivity in Lancaster Sound and approaches during the summer of 1979, Technical report 423, Canadian Data Report of Fisheries and Aquatic Sciences, 1984.

Irwin, B., Caverhill, C., Harrison, W. G., and Platt, T.: Primary production in the Sargasso Sea northeast of Bermuda in April 1984, Technical report 550, Canadian Data Report of Fisheries and Aquatic Sciences, 1985.

https://doi.org/10.5194/essd-2026-651
Preprint. Discussion started: 25 August 2026

Irwin, B., Caverhill, C., Dickie, P., Hodgson, M., and Platt, T.: Primary productivity of ice algae on the Labrador Shelf from March 16 to March 27, 1984, Technical report 559, Canadian Data Report of Fisheries and Aquatic Sciences, 1986a.

Irwin, B., Caverhill, C., Dickie, P., Horne, E., and Platt, T.: Primary productivity on the Labrador Shelf during June and July 1984, Technical report 577, Canadian Data Report of Fisheries and Aquatic Sciences, 1986b.

Irwin, B., Caverhill, C., and Platt, T.: Primary production on the Grand Banks of Newfoundland in April 1984, Technical report 579, Canadian Data Report of Fisheries and Aquatic Sciences, 1986c.

Irwin, B., Platt, T., and Caverhill, C.: Primary productivity and other related measurements in Eastern Canadian Arctic during the summer of 1983, Technical report 510, Canadian Data Report of Fisheries and Aquatic Sciences, 1986d.

Irwin, B., Caverhill, C., Anning, J., Mossman, D., and Platt, T.: Primary production on Georges Bank in the Northern Sargasso Sea in July and August 1985, Technical report 670, Canadian Data Report of Fisheries and Aquatic Sciences, 1987a.

Irwin, B., Caverhill, C., Anning, J., and Platt, T.: Primary production and related measurements at a fixed station in the Caribbean Sea in December 1984, Technical report 671, Canadian Data Report of Fisheries and Aquatic Sciences, 1987b.

Irwin, B., Horne, E., Boulding, E. P. W., and Platt, T.: Phytoplankton productivity in Jones Sound during August and September, 1984, Technical report 676, Canadian Data Report of Fisheries and Aquatic Sciences, 1987c.

Irwin, B., Caverhill, C., Anning, J., Mossman, D., and Platt, T.: Carbon and oxygen primary production in Bedford Basin, Nova Scotia from March to June 1985, Technical report 686, Canadian Data Report of Fisheries and Aquatic Sciences, 1988a.

Irwin, B., Caverhill, C., Platt, T., and Fasham, M. J.: Primary production in the Celtic Sea in May and June 1986, Technical report 718, Canadian Data Report of Fisheries and Aquatic Sciences, 1988b.

Irwin, B., Dickie, P., Hodgson, M., and Platt, T.: Primary production and nutrients on the Labrador Shelf, in Hudson Strait and Hudson Bay in August and September 1982, Technical report 692, Canadian Data Report of Fisheries and Aquatic Sciences, 1988c.

Irwin, B., Harrison, W. G., Anning, J., Caverhill, C., Dickie, P., and Platt, T.: Phytoplankton production and distribution on the Grand Banks of Newfoundland in September 1985, Technical report 691, Canadian Data Report of Fisheries and Aquatic Sciences, 1988d.

Irwin, B., Caverhill, C., Anning, J., and MacDonald, A.: Productivity Localised Around Seamounts in the Atlantic (PLASMA) during June and July 1987, Technical report 732, Canadian Data Report of Fisheries and Aquatic Sciences, 1989a.

Irwin, B., Caverhill, C., Mossman, D., Anning, J., Horne, E., and Platt, T.: Primary productivity on the Labrador Shelf during July 1985, Technical report 760, Canadian Data Report of Fisheries and Aquatic Sciences, 1989b.

Irwin, B., Anning, J., Caverhill, C., Hodgson, M., MacDonald, A., and Platt, T.: Primary production in the Northern Sargasso Sea in September 1988, Technical report 798, Canadian Data Report of Fisheries and Aquatic Sciences, 1990a.

Irwin, B., Anning, J., Caverhill, C., MacDonald, A., and Platt, T.: Primary production on Georges Bank—August 1988, Technical report 785, Canadian Data Report of Fisheries and Aquatic Sciences, 1990b.

Irwin, B., Anning, J., Caverhill, C., and Platt, T.: Primary production on the Labrador Shelf and in the Strait of Belle Isle in May 1988, Technical report 784, Canadian Data Report of Fisheries and Aquatic Sciences, 1990c.

https://doi.org/10.5194/essd-2026-651
Preprint. Discussion started: 25 August 2026

Open Access Earth System Science Data Discussions

Jassby, A. D. and Platt, T.: Mathematical formulation of the relationship between photosynthesis and light for phytoplankton, Limnology and oceanography, 21, 540–547, 1976.

Kam, K., Devred, E., Clay, S., Amirian, M. M., Irwin, A., Atamanchuk, D., Send, U., and Wallace, D. W.: Resolving satellite-in situ mismatches in Net Primary Production using high-frequency in situ bio-optical observations in the subpolar Northwest Atlantic, arXiv preprint arXiv:2604.08634, 2026.

Kovač, Ž., Platt, T., Sathyendranath, S., and Antunović, S.: Models for estimating photosynthesis parameters from in situ production profiles, Progress in oceanography, 159, 255–266, 2017.

Kovač, Ž., Platt, T., Ninčević Gladan, Ž., Morović, M., Sathyendranath, S., Raitsos, D. E., Grbec, B., Matić, F., and Veža, J.: A 55-year time series station for primary production in the Adriatic Sea: data correction, extraction of photosynthesis parameters and regime shifts, Remote Sensing, 10, 1460, 2018.

Kovač, Ž., Bačeković Koloper, M., Sathyendranath, S., Kulk, G., Bouman, H., and Ćatipović, L.: A new global dataset of photosynthesis parameters, Earth System Science Data Discussions, 2026, 1–23, 2026.

Kulk, G., Platt, T., Dingle, J., Jackson, T., Jönsson, B. F., Bouman, H. A., Babin, M., Brewin, R. J., Doblin, M., Estrada, M., et al.: Primary production, an index of climate change in the ocean: satellite-based estimates over two decades, Remote Sensing, 12, 826, 2020.

Kyewalyanga, M. N., Platt, T., and Sathyendranath, S.: Estimation of the photosynthetic action spectrum: implication for primary production models, Marine Ecology Progress Series, 146, 207–223, 1997.

Lipsey, M. W. and Wilson, D. B.: Practical meta-analysis., SAGE publications, Inc, 2001.

Longhurst, A., Sathyendranath, S., Platt, T., and Caverhill, C.: An estimate of global primary production in the ocean from satellite radiometer data, Journal of plankton Research, 17, 1245–1271, 1995.

Longhurst, A. R.: Ecological geography of the sea, Elsevier, 2010.

Mattei, F. and Scardi, M.: Collection and analysis of a global marine phytoplankton primary production dataset, Earth System Science Data Discussions, 2021, 1–29, 2021.

McKinley, G. A., Fay, A. R., Lovenduski, N. S., and Pilcher, D. J.: Natural variability and anthropogenic trends in the ocean carbon sink, Annual review of marine science, 9, 125–150, 2017.

Mullin, T. B. and Riley, J. P.: The Colorimetric Determination of Silicate with Special Reference to Sea and Natural Waters, Analytica Chimica Acta, 12, 162–176, 1955.

Murphy, J. and Riley, J. P.: A Modified Single Solution Method for the Determination of Phosphate in Natural Waters, Analytica Chimica Acta, 27, 31–36, 1962.

Neale, P. J. and Richerson, P. J.: Photoinhibition and the diurnal variation of phytoplankton photosynthesis—I. Development of a photosynthesis—irradiance model from studies of in situ responses, Journal of Plankton Research, 9, 167–193, 1987.

Oehlert, G. W.: A note on the delta method, The American Statistician, 46, 27–29, 1992.

Peeters, J. and Eilers, P.: The relationship between light intensity and photosynthesis—a simple mathematical model, Hydrobiological Bulletin, 12, 134–136, 1978.

Platt, T. and Sathyendranath, S.: Oceanic primary production: estimation by remote sensing at local and regional scales, Science, 241, 1613–1620, 1988.

Platt, T., Gallegos, C. L., and Harrison, W. G.: Photoinhibition of photosynthesis in natural assemblages of marine phytoplankton, Journal of Marine Research, 1980.

Prioul, J. and Chartier, P.: Partitioning of transfer and carboxylation components of intracellular resistance to photosynthetic CO2 fixation: a critical analysis of the methods used, Annals of Botany, 41, 789–800, 1977.

https://doi.org/10.5194/essd-2026-651
Preprint. Discussion started: 25 August 2026

Sathyendranath, S., Platt, T., Kovač, Ž., Dingle, J., Jackson, T., Brewin, R. J., Franks, P., Marañón, E., Kulk, G., and Bouman, H. A.: Reconciling models of primary production and photoacclimation, Applied Optics, 59, C100–C114, 2020.

Sharoni, S., Inomura, K., Dutkiewicz, S., Jahn, O., Finkel, Z. V., Irwin, A., M. Amirian, M., Monier, E., and Follows, M. J.: Biochemical remodelling of phytoplankton cell composition under climate change, Nature Climate Change, pp. 1–7, 2026.

Smith, E. L.: Photosynthesis in relation to light and carbon dioxide, Proceedings of the National Academy of Sciences, 22, 504–511, 1936.

Solorzano, L.: Determination of Ammonia in Natural Waters by the Phenolhypochlorite Method, Limnology and Oceanography, 14, 799–801, 1969.

Steele, J. H.: Environmental control of photosynthesis in the sea, Limnology and oceanography, 7, 137–150, 1962.

Strickland, J. D. H. and Parsons, T. R.: A Practical Handbook of Seawater Analysis, vol. 167 of *Bulletin of the Fisheries Research Board of Canada*, Fisheries Research Board of Canada, 2 edn., 1972.

Tagliabue, A., Kwiatkowski, L., Bopp, L., Butenschön, M., Cheung, W., Lengaigne, M., and Vialard, J.: Persistent uncertainties in ocean net primary production climate change projections at regional scales raise challenges for assessing impacts on ecosystem services, Frontiers in Climate, 3, 738 224, 2021.

Tréguer, P., Bowler, C., Moriceau, B., Dutkiewicz, S., Gehlen, M., Aumont, O., Bittner, L., Dugdale, R., Finkel, Z., Iudicone, D., et al.: Influence of diatom diversity on the ocean biological carbon pump, Nature Geoscience, 11, 27–37, 2018.

Webb, W. L., Newton, M., and Starr, D.: Carbon dioxide exchange of Alnus rubra, Oecologia, 17, 281–291, 1974.

Westberry, T. K., Silsbe, G. M., and Behrenfeld, M. J.: Gross and net primary production in the global ocean: An ocean color remote sensing perspective, Earth-Science Reviews, 237, 104 322, 2023.

Westwood, K. J., Griffiths, F. B., Webb, J. P., and Wright, S. W.: Primary production in the Sub-Antarctic and Polar Frontal zones south of Tasmania, Australia; SAZ-Sense survey, 2007, Deep Sea Research Part II: Topical Studies in Oceanography, 58, 2162–2178, 2011.

Yentsch, C. S. and Menzel, D. W.: A Method for the Determination of Phytoplankton Chlorophyll and Phaeophytin by Fluorescence, Deep-Sea Research, 10, 221–231, 1963.